Research article

Balancing mitigation strategies for viral outbreaks

Hamed Karami, Pejman Sanaei and Alexandra Smirnova[*]

Department of Mathematics & Statistics, Georgia State University, Atlanta, USA

* **Correspondence:** Email: asmirnova@gsu.edu.

Abstract: Control and prevention strategies are indispensable tools for managing the spread of infectious diseases. This paper examined biological models for the post-vaccination stage of a viral outbreak that integrate two important mitigation tools: social distancing, aimed at reducing the disease transmission rate, and vaccination, which boosts the immune system. Five different scenarios of epidemic progression were considered: (i) the "no control" scenario, reflecting the natural evolution of a disease without any safety measures in place, (ii) the "reconstructed" scenario, representing real-world data and interventions, (iii) the "social distancing control" scenario covering a broad set of behavioral changes, (iv) the "vaccine control" scenario demonstrating the impact of vaccination on epidemic spread, and (v) the "both controls concurrently" scenario incorporating social distancing and vaccine controls simultaneously. By comparing these scenarios, we provided a comprehensive analysis of various intervention strategies, offering valuable insights into disease dynamics. Our innovative approach to modeling the cost of control gave rise to a robust computational algorithm for solving optimal control problems associated with different public health regulations. Numerical results were supported by real data for the Delta variant of the COVID-19 pandemic in the United States.

Keywords: epidemiology; compartmental model; transmission dynamic; optimal control

1. Introduction

Control and elimination of infectious diseases have been a focus of public health officials since the early 1950s. As antibiotics [1, 2], sanitation [3], and vaccinations [4–6] were introduced, eradicating diseases became more feasible [7, 8]. Nevertheless, several factors have led to the emergence of new infectious diseases and the reemergence of existing ones, including resistance of microorganisms to medication [9–11], demographic evolution [12], urbanization [13, 14], and increased travel [15]. These diseases include Lyme disease in 1975 [16], Legionnaires disease in 1976 [17], toxic shock syndrome in 1978 [18], Hepatitis C in 1989 [19], Hepatitis E in 1990 [20], and Hantavirus in 1993 [21]. HIV (human immunodeficiency virus) emerged in 1981 as one of the most alarming sexually transmitted

diseases in the world [22, 23]. As the result of antibiotic resistance, tuberculosis, pneumonia, and gonorrhea are reemerging [24]. Because of climate change, malaria, dengue, and yellow fever have also reemerged and are spreading into new areas [25]. Moreover, it is not unusual for diseases such as plague and cholera to erupt from time to time [26]. The reemergence of the Ebola virus disease (EVD) in 2013 has puzzled the world [27]. Fifteen million deaths are directly related to the reemergence of infectious diseases every year, which remains a serious medical burden around the globe [28, 29].

In the field of epidemiology, the application of optimal control strategies has proven to be a critical tool in managing and mitigating the spread of infectious diseases [30–32]. Optimal control theory provides a robust framework that allows one to incorporate one or more time-dependent control functions into a nonlinear dynamic system to achieve the best possible outcome for a specified objective [33, 34]. It uses mathematical and computational techniques aimed at identifying the most effective interventions, such as vaccination [35], treatment plans [36], quarantines, and social distancing [37], while optimizing the use of resources [38, 39]. By integrating optimal control into disease models, researchers can predict and influence the progression of an outbreak, ultimately reducing morbidity, mortality, and economic impact [40–42].

Optimal control problems have been extensively studied across various infectious diseases. For instance, during the 2014–2016 Ebola outbreak in West Africa, optimal control models were developed to evaluate the effectiveness of different intervention strategies, including isolation [43], contact tracing [44], and public health campaigns [45, 46]. Dengue fever, a mosquito-borne viral disease, also presents a significant public health challenge in tropical and subtropical regions [47]. Optimal control strategies for dengue have focused on reducing mosquito populations and limiting human exposure through targeted insecticide use [48], environmental management [49], and vaccination [50, 51]. The COVID-19 pandemic has brought the application of optimal control strategies to the forefront of public health efforts globally [34, 52]. Researchers have developed models to determine the best combination of non-pharmaceutical interventions (NPIs) such as social distancing [53], lockdowns [54], and mask-wearing [55], alongside vaccination rollouts [54, 56]. These models have been instrumental in guiding policy decisions, helping to balance the trade-offs between controlling the virus and minimizing societal disruption [57–59]. Other diseases, such as influenza [60, 61], malaria [62], Zika virus [63], various types of cancer, and HIV [64], have also been the focus of optimal control studies, each contributing to the development of a robust framework for disease management [65, 66].

In this paper, we develop a robust optimal control algorithm to simulate five epidemic scenarios: "no control", "reconstructed", "social distancing control", "vaccine control", and "both controls concurrently", using biological models for the post-vaccination stage of a viral outbreak. For numerical validation, we employ real data for the SARS-CoV-2 Delta variant in different regions of the United States of America from July 9, 2021 to November 25, 2021. By comparing several control scenarios, we provide an overarching study of crucial intervention strategies, offering valuable insights into disease transmission. Our innovative approach to modeling the cost of control gives rise to a fast trust-region optimization procedure for solving a broad range of nonlinear control problems.

The paper is organized as follows: Section 2 outlines mathematical preliminaries essential to our analysis. We introduce and examine the social distancing control strategy in Section 3. In Section 4, the vaccine control is investigated, and Section 5 is dedicated to the combined implementation of social distancing and vaccination controls. In Section 6, we compare the aforementioned scenarios and assess their efficiency. Additional figures and tables are presented in the Appendix.

2. Mathematical preliminaries

Mathematical models have been extensively used to analyze the spread of infectious diseases, such as Ebola, dengue, plague, influenza, and COVID-19, and to forecast their impact [67, 68]. Disease models range in complexity from basic Susceptible - Exposed - Infectious - Recovered (SEIR) ODE systems with few parameters to more sophisticated models that include numerous compartments and parameters to account for isolation [69], hospitalization, testing, contact tracing [70], social distancing [71, 72], vaccination [73], and others [74, 75]. In this study, we consider the $\hat{S}_u \hat{S}_v \hat{I}_u \hat{I}_v \hat{R} \hat{D}$ compartmental model that was first introduced in [76] and further studied in [77]:

$$
\begin{aligned}
\frac{d\hat{S}_u}{dt} &= -\zeta(t)\frac{\hat{S}_u(t)}{N - \hat{D}(t)}(\hat{I}_u(t) + \hat{I}_v(t)) - \mu\hat{S}_u(t) + \delta_r\hat{R}(t) + \delta_v\hat{S}_v(t), \\
\frac{d\hat{S}_v}{dt} &= -(1 - \alpha)\zeta(t)\frac{\hat{S}_v(t)}{N - \hat{D}(t)}(\hat{I}_u(t) + \hat{I}_v(t)) + \mu\hat{S}_u(t) - \delta_v\hat{S}_v(t), \\
\frac{d\hat{I}_u}{dt} &= \zeta(t)\frac{\hat{S}_u(t)}{N - \hat{D}(t)}(\hat{I}_u(t) + \hat{I}_v(t)) - (\gamma_{u,r} + \gamma_{u,d})\hat{I}_u(t), \\
\frac{d\hat{I}_v}{dt} &= (1 - \alpha)\zeta(t)\frac{\hat{S}_v(t)}{N - \hat{D}(t)}(\hat{I}_u(t) + \hat{I}_v(t)) - (\gamma_{v,r} + \gamma_{v,d})\hat{I}_v(t), \\
\frac{d\hat{R}}{dt} &= \gamma_{u,r}\hat{I}_u(t) + \gamma_{v,r}\hat{I}_v(t) - \delta_r\hat{R}(t), \\
\frac{d\hat{D}}{dt} &= \gamma_{u,d}\hat{I}_u(t) + \gamma_{v,d}\hat{I}_v(t).
\end{aligned}
\tag{2.1}
$$

This model incorporates the vaccination status of both susceptible and infected individuals, as well as the possibility of losing immunity and becoming infected among both vaccinated and unvaccinated populations [76]. Epidemic model (2.1) has 6 compartments: Susceptible unvaccinated ($\hat{S}_u$), Susceptible vaccinated ($\hat{S}_v$), Infected unvaccinated ($\hat{I}_u$), Infected vaccinated ($\hat{I}_v$), Recovered ($\hat{R}$), and Deceased ($\hat{D}$). In (2.1), the time-dependent parameter, $\zeta(t)$, is the disease transmission rate, μ is the average vaccination rate, δ_r is the rate at which individuals lose immunity after acquiring the virus, δ_v is the waning vaccine immunity rate, and $\gamma_{u,r}$ and $\gamma_{v,r}$ are the recovery rates for unvaccinated and vaccinated individuals, respectively. The virus death rates for unvaccinated and vaccinated humans are denoted by $\gamma_{u,d}$ and $\gamma_{v,d}$, and α ($0 < \alpha < 1$) is the measure of vaccine efficacy for the current strain. In the above, $t \in [0, T]$, where T is the length of the study period.

In model (2.1), it is assumed that the duration of each virus strain is relatively short compared to the time it takes for the population to change due to birth, migration, death of causes rather than the virus, etc. Therefore natural birth and death are omitted in the model, and we assume that at any given time, t, the population of the region is $N - D(t)$, where N is the population at $t = 0$, that is, $N = \hat{S}_u(0) + \hat{S}_v(0) + \hat{I}_u(0) + \hat{I}_v(0) + \hat{R}(0) + \hat{D}(0)$. We also assume that vaccination is applied only to susceptible individuals, and infected and recovered individuals are not vaccinated until they lose immunity and move back to the susceptible class. So, this model does not account for asymptomatic infected individuals that can be vaccinated while still infected or in the recovered stage. According to model (2.1), the loss of immunity after infection is the same for both vaccinated and unvaccinated individuals.

In ODE system (2.1), $\zeta(t)$ is a time-dependent parameter that accounts for real-life nonmedical preventive measures (social distancing, bans on travel and large gatherings, handwashing, etc.) aimed at bringing down the disease transmission. In our numerical simulations, $\zeta(t)$ is reconstructed for individual states from real data on new incidence cases and daily deaths [78] using the algorithm proposed in [77]. Another important parameter, μ, is the average vaccination rate, which is pre-estimated based on CDC reports [76, 79] (for individual states) by dividing the change in the percentage of vaccinated people at the start and at the end of the study window by the length of this window. As proposed in [76, 80, 81], we assume that susceptible unvaccinated individuals move to the susceptible vaccinated class at the rate proportional to the current number of susceptible unvaccinated individuals. By estimating $\zeta(t)$ and μ in this manner, we analyze the *actual* disease progression (what is called the "reconstructed" scenario in our experiments).

The goal of the optimal control problem is to see how much the real-life scenario can be improved through the implementation of control strategies that optimize a specific objective functional. To that end, in the "real-life" model (2.1), we replace $\zeta(t)$ with $\beta(1 - u_1(t))$, where β is the original disease transmission rate and $u_1(t)$ is the social distancing control that we aspire to optimize. Clearly, one has $\beta \geq \max_{t \in [0,T]} \zeta(t)$ since $\zeta(t) = \beta(1 - \tilde{u}_1(t))$, where $\tilde{u}_1(t)$ is a "real-life" non-optimal social distancing control ($0 \leq \tilde{u}_1(t) < 1$ for $t \in [0, T]$). In order to facilitate the vaccination strategy, we replace μ with $\nu u_2(t)$, where $\nu > \mu$ is the capacity of vaccination and $u_2(t)$ is the vaccination control. The feasible set for $u_1(t)$ and $u_2(t)$ is

$$\mathcal{U} = \left\{ u_i \in \mathcal{L}^1[0, T], \quad 0 \leq u_i(t) < 1, \quad i = 1, 2 \right\}. \tag{2.2}$$

To simplify the biological model, we normalize the state variables, $S_u := \frac{\hat{S}_u}{N}$, $S_v := \frac{\hat{S}_v}{N}$, $I_u := \frac{\hat{I}_u}{N}$, $I_v := \frac{\hat{I}_v}{N}$, $R := \frac{\hat{R}}{N}$, and $D := \frac{\hat{D}}{N}$, and arrive at the following controlled system of differential equations:

$$
\begin{aligned}
\frac{dS_u}{dt} &= -\beta(1 - u_1(t))\frac{S_u(t)}{1 - D(t)}(I_u(t) + I_v(t)) - \nu u_2(t)S_u(t) + \delta_r R(t) + \delta_v S_v(t), \\
\frac{dS_v}{dt} &= -(1 - \alpha)\beta(1 - u_1(t))\frac{S_v(t)}{1 - D(t)}(I_u(t) + I_v(t)) + \nu u_2(t)S_u(t) - \delta_v S_v(t), \\
\frac{dI_u}{dt} &= \beta(1 - u_1(t))\frac{S_u(t)}{1 - D(t)}(I_u(t) + I_v(t)) - (\gamma_{u,r} + \gamma_{u,d})I_u(t), \\
\frac{dI_v}{dt} &= (1 - \alpha)\beta(1 - u_1(t))\frac{S_v(t)}{1 - D(t)}(I_u(t) + I_v(t)) - (\gamma_{v,r} + \gamma_{v,d})I_v(t), \\
\frac{dR}{dt} &= \gamma_{u,r}I_u(t) + \gamma_{v,r}I_v(t) - \delta_r R(t), \\
\frac{dD}{dt} &= \gamma_{u,d}I_u(t) + \gamma_{v,d}I_v(t).
\end{aligned}
\tag{2.3}
$$

The two control functions, $u_1(t)$ and $u_2(t)$, are intended to lower the normalized force of infection, $\beta(1 - u_1(t))\frac{S_u(t) + (1-\alpha)S_v(t)}{1 - D(t)}(I_u(t) + I_v(t))$, while keeping the costs at bay. The costs of control are understood in a general sense, which includes a negative impact on the economy, mental health, education, and other aspects of life [82]. With that in mind, we propose the following objective functional

$$J(\mathbf{x}, \mathbf{u}) = \int_0^T \left\{ \beta(1 - u_1(t))\frac{S_u(t) + (1 - \alpha)S_v(t)}{1 - D(t)}(I_u(t) + I_v(t)) + \lambda^\top \mathbf{c}(\mathbf{u}(t)) \right\} dt$$

$$= (S_u + S_v)(0) - (S_u + S_v)(T) + \int_0^T \left\{ \boldsymbol{\lambda}^\top \mathbf{c}(\mathbf{u}(t)) + \delta_r R(t) \right\} dt, \tag{2.4}$$

where $\mathbf{x}(t) := [S_u(t), S_v(t), I_u(t), I_v(t), R(t), D(t)]^\top$ combines all normalized state variables of the model, $\boldsymbol{u}(t) := [u_1(t), u_2(t)]^\top$ represents the two control strategies, $\mathbf{c}(\mathbf{u}) := [c_1(u_1), c_2(u_2)]^\top$ stands for the vector of cost functions associated with $u_1(t)$ and $u_2(t)$, respectively, and $\boldsymbol{\lambda} := [\lambda_1, \lambda_2]^\top$ is the weight vector for the cost functions, $c_i(u_i)$, $i = 1, 2$. Thus, the optimal control problem for what we call the "both controls concurrently" scenario is to minimize objective functional (2.4) subject to ODE system (2.3).

In the next two sections, we will also introduce two special cases, "social distancing control" (i.e., social distancing control only) and "vaccine control" (i.e., vaccine control only), with functional (2.4) and model (2.3) adjusted accordingly. Numerical results for these three control problems will be compared with the aforementioned "reconstructed" scenario (2.1) and with the "no control" scenario, described by $S_u I_u RD$ model (2.5) below. To introduce the "no control" disease progression, we assume that neither social distancing nor vaccination control is enforced, that is, the epidemic is running its course. Hence, the disease transmission rate is constant (and equal to β) and there are no vaccinated compartments for either susceptible or infected humans:

$$\begin{aligned}
\frac{dS_u}{dt} &= -\beta \frac{S_u(t)I_u(t)}{1 - D(t)} + \delta_r R(t), \\
\frac{dI_u}{dt} &= \beta \frac{S_u(t)I_u(t)}{1 - D(t)} - (\gamma_{u,r} + \gamma_{u,d})I_u(t), \\
\frac{dR}{dt} &= \gamma_{u,r} I_u(t) - \delta_r R(t), \\
\frac{dD}{dt} &= \gamma_{u,d} I_u(t).
\end{aligned} \tag{2.5}$$

According to Pontryagin's Minimum Principle [33, 83], if $\mathbf{u} \in \mathcal{U}$ is an optimal control strategy with respect to the objective functional $J(\mathbf{x}, \mathbf{u}) = h(\mathbf{x}(T)) + \int_0^T L(\mathbf{x}(t), \mathbf{u}(t)) \, dt$ and the system of equations $\dot{\mathbf{x}} = f(\mathbf{x}, \mathbf{u})$, $\mathbf{x}(0) = \mathbf{x_0}$, then there is a trajectory $\mathbf{p}(t)$ such that

$$\dot{\mathbf{p}}(t) = -\partial_\mathbf{x} H(\mathbf{x}, \mathbf{u}, \mathbf{p})^\top \big|_{\mathbf{x}(t), \mathbf{u}(t), \mathbf{p}(t)}, \quad \mathbf{p}(T) = \partial_\mathbf{x} h(\mathbf{x})^\top \big|_{\mathbf{x}(T)}, \tag{2.6}$$

$$\mathbf{u}(t) = \underset{\mathbf{v} \in \mathcal{U}}{\arg\min} \, H(\mathbf{x}(t), \mathbf{v}(t), \mathbf{p}(t)), \quad H(\mathbf{x}, \mathbf{v}, \mathbf{p}) := L(\mathbf{x}, \mathbf{v}) + \mathbf{p}^\top f(\mathbf{x}, \mathbf{v}). \tag{2.7}$$

Therefore, solving the optimal control problems for the "social distancing control", "vaccine control", and "both controls concurrently" scenarios comes down to minimizing the Hamiltonian, $H(\mathbf{x}, \mathbf{u}, \mathbf{p})$, with respect to $\mathbf{u}$ subject to costate system (2.6) and the biological model $\dot{\mathbf{x}} = f(\mathbf{x}, \mathbf{u})$, $\mathbf{x}(0) = \mathbf{x_0}$. The complexity of this minimization problem largely depends on the choice of the cost function, $\mathbf{c}(\mathbf{u})$, in the objective functional (2.4). In our algorithms, we employ a twice continuously differentiable cost function, $\mathbf{c}(\mathbf{u}) := [c_1(u_1), c_2(u_2)]^\top$, with the following key properties [82]:

- $c_i(u)$, $i = 1, 2$, are defined in $\mathcal{D}_i \supseteq [0, 1)$ ensuring that each domain contains the feasible set;
- $c_i(0) = 0$, $i = 1, 2$, implying zero cost when no control is applied;
- $\lim_{u \to 1^-} c_i(u) = \infty$, guaranteeing that the cost becomes prohibitive as u approaches the upper bound of the control range;

- $c_i'(u) > 0$ when $u > 0$, and $c_i'(u) < 0$ when $u < 0$, suggesting that $c_i(u)$ is increasing for positive control values and preventing u from becoming negative;
- $c_i''(u) > 0$ for all $u \in \mathcal{D}_i$, indicating that $c_i(u)$ is strictly convex, $i = 1, 2$.

Note that $c_i(u)$, $i = 1, 2$, satisfying the above conditions, are necessarily nonnegative in their respective domains, $\mathcal{D}_i$. In the numerical simulations presented in this paper, for different control scenarios, we consider the following four cost functions, $i = 1, 2$ [84]:

$$c_{i,1}(u) = -u - \ln(1 - u), \; c_{i,2}(u) = u^2, \; c_{i,3}(u) = -\ln(1 - u^2), \; c_{i,4}(u) = -u\ln(1 - u). \quad (2.8)$$

It is important to mention that for $c_{i,2}(u) = u^2$ [85, 86], which is often used in optimal control problems (or for a more general function, $c_{i,2}(u) = w_1 u + w_2 u^2$ [87, 88]), the requirement $\lim_{u \to 1^-} c_i(u) = \infty$ is not met. In our experimental framework, $c_{i,2}(u) = u^2$, $i = 1, 2$, is used for comparison to highlight the importance of the property $\lim_{u \to 1^-} c_i(u) = \infty$. For $c_{i,1}$, $c_{i,3}$, and $c_{i,4}$, all assumptions listed above are fulfilled and, as our experiments show, all candidates for the global minimum of $H(\mathbf{x}, \mathbf{u}, \mathbf{p})$ with respect to $\mathbf{u}$ subject to the state and costate systems are feasible, i.e., inequality constraints, $u_i \geq 0$ and $u_i < 1$ (or control-specific constraint, $u_i < b_i$ [87, 88]), do not have to be enforced in the optimization algorithm. This is not the case with $c_{i,2}(u) = u^2$. For this cost function, one or both coordinates of the global minimum are often greater than 1, especially for small values of λ_i. The details are presented in Sections 3–5.
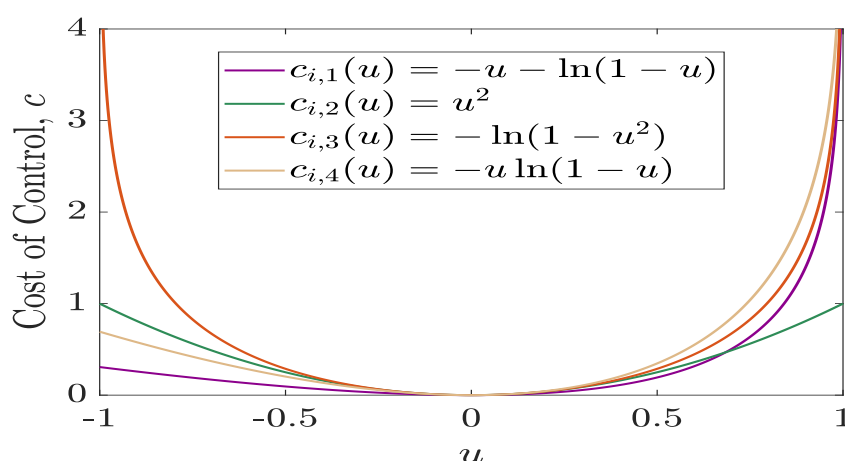

Figure 1. The graph of cost functions $c_{i,j}$, $j = 1, 2, 3, 4$, where $c_{1,j}$ stands for the cost of social distancing control, $u_1(t)$, and $c_{2,j}$ refers to the cost of vaccination control, $u_2(t)$.

For the three optimal control problems "social distancing control", "vaccine control", and "both controls concurrently", investigated in Sections 3–5, respectively, we use $c_{1,j}(u) = c_{2,j}(u)$, $j = 1, 2, 3, 4$. However, in some applications, the cost functions associated with different controls may need to be different. The computational algorithm can easily be adapted for that. The graphs of the cost functions, $c_{i,j}(u)$, $u \in [-1, 1)$, $i = 1, 2$, $j = 1, 2, 3, 4$, are shown in Figure 1.

3. Social distancing control

In this section, we consider an intervention scenario where only social distancing controls are implemented. Similar to (2.5), there are no vaccinated compartments for either susceptible or infected

humans, and the model with social distancing control, $u_1(t) \in \mathcal{U}$, takes the form:

$$
\begin{aligned}
\frac{\mathrm{d}S_u}{dt} &= -\beta(1 - u_1(t))\frac{S_u(t)I_u(t)}{1 - D(t)} + \delta_r R(t), \\
\frac{\mathrm{d}I_u}{dt} &= \beta(1 - u_1(t))\frac{S_u(t)I_u(t)}{1 - D(t)} - (\gamma_{u,r} + \gamma_{u,d})I_u(t), \\
\frac{\mathrm{d}R}{dt} &= \gamma_{u,r}I_u(t) - \delta_r R(t), \\
\frac{\mathrm{d}D}{dt} &= \gamma_{u,d}I_u(t).
\end{aligned}
\tag{3.1}
$$

A higher control value implies more strict social distancing measures, leading to a reduced transmission. On the other hand, $u_1(t) = 0$ yields no social distancing and a disease transmission rate reaching its full potential. With no vaccination control, the normalized force of infection is $\beta(1 - u_1(t))\frac{S_u(t)I_u(t)}{1 - D(t)}$, and one arrives at the following objective functional:

$$
\begin{aligned}
J(\mathbf{x}, u_1) &= \int_0^T \left\{ \beta(1 - u_1(t))\frac{S_u(t)I_u(t)}{1 - D(t)} + \lambda_1 c_1(u_1(t)) \right\} \mathrm{d}t \\
&= S_u(0) - S_u(T) + \int_0^T \{\lambda_1 c_1(u_1(t)) + \delta_r R(t)\} \, \mathrm{d}t,
\end{aligned}
\tag{3.2}
$$

designed to achieve a balance between reducing the spread of the disease and managing the associated mitigation costs over the period $[0, T]$. In (3.2), $\mathbf{x} := [S_u, I_u, R, D]^\top$. Equations (2.7), (3.1), and (3.2) give rise to the Hamiltonian:

$$
\begin{aligned}
H(\mathbf{x}, u_1, \mathbf{p}) = {}& \lambda_1 c_1(u_1) + \delta_r R + p_1 \left[-\beta(1 - u_1)\frac{S_u I_u}{1 - D} + \delta_r R \right] \\
&+ p_2 \left[\beta(1 - u_1)\frac{S_u I_u}{1 - D} - (\gamma_{u,r} + \gamma_{u,d})I_u \right] + p_3 \left(\gamma_{u,r}I_u - \delta_r R \right) + p_4 \, \gamma_{u,d}I_u,
\end{aligned}
\tag{3.3}
$$

where $\mathbf{p} := [p_1, p_2, p_3, p_4]^\top$. By Pontryagin's Minimum Principle [33, 83], $u_1 = \arg \min_{v \in \mathcal{U}} H(\mathbf{x}, v, \mathbf{p})$, subject to state system (3.1) and costate system (2.6) in the form

$$
\begin{aligned}
\frac{dp_1}{dt} &= \frac{\beta(1 - u_1(t))}{1 - D(t)}I_u(t)(p_1(t) - p_2(t)), \\
\frac{dp_2}{dt} &= \frac{\beta(1 - u_1(t))}{1 - D(t)}S_u(t)(p_1(t) - p_2(t)) + \gamma_{u,r}(p_2(t) - p_3(t)) + \gamma_{u,d}(p_2(t) - p_4(t)), \\
\frac{dp_3}{dt} &= \delta_r(p_3(t) - p_1(t) - 1), \\
\frac{dp_4}{dt} &= \frac{\beta(1 - u_1(t))}{(1 - D(t))^2}S_u(t)I_u(t)(p_1(t) - p_2(t)), \quad \mathbf{p}(T) = [-1, 0, 0, 0]^\top.
\end{aligned}
\tag{3.4}
$$

This leads to the following 2nd-order numerical algorithm for nonlinear constrained minimization:

Algorithm 1 Numerical method for solving the social distancing optimal control problem

Require: Cost function $c_{1,j}(u_1)$, weight λ_1, finite dimensional approximation $u_1[\theta]$, initial guess θ.
Ensure: Optimal control $u_1[\theta]$ with estimated θ.
   repeat
       Solve (3.1) for **x** forward in time.
       Solve (3.4) for **p** backward in time.
       $\theta \leftarrow \theta - \varrho(J^\top(\theta)J(\theta) + \omega_k I)^{-1}J^\top(\theta)F(\theta)$.
   until converged.

In Algorithm 1, $F(\theta)$ is a discrete analog of the partial derivative of the Hamiltonian, $H(\mathbf{x}, u_1, \mathbf{p})$, with respect to u_1, $J(\theta)$ is the Jacobian of $F(\theta)$, I is the identity matrix in the solution space, ϱ is the step size, and ω_k is the regularization sequence. The derivative of $H(\mathbf{x}, u_1, \mathbf{p})$ with respect to u_1 exists, since $c_{1,j}(u)$, $j = 1, 2, 3, 4$, are twice continuously differentiable by our assumption. In all our experiments, shifted Legendre polynomials were used to project the control function, $u_1(t)$, onto a finite dimensional subspace with θ being a vector of expansion coefficients. MATLAB's built-in function "ode15s" was employed to solve both ODE systems, (3.1) and (3.4), while "lsqnonlin" implemented the Levenberg-Marquardt optimization procedure.
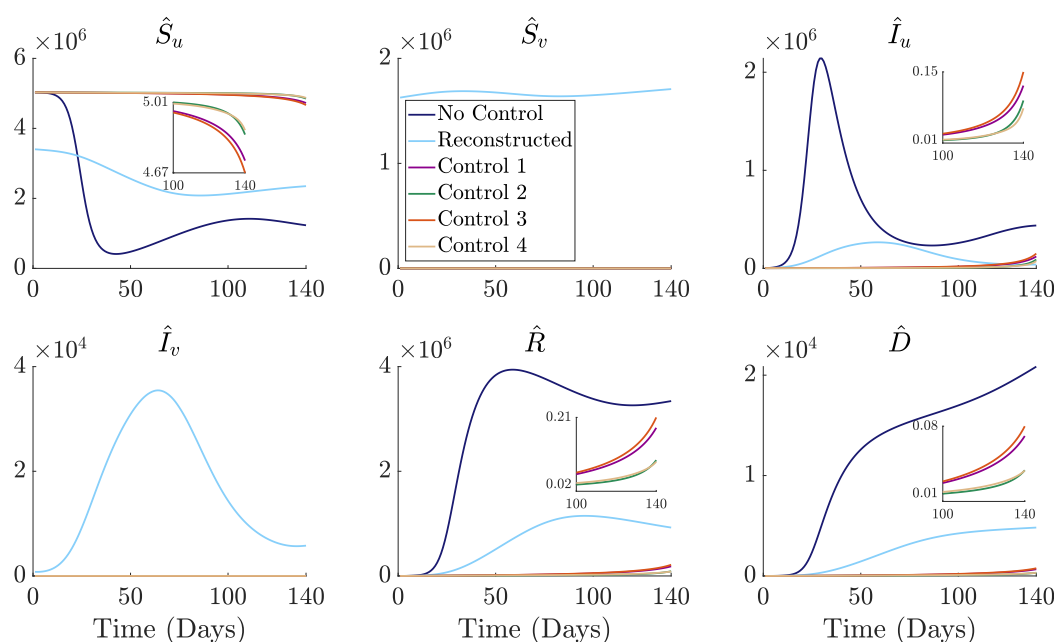

Figure 2. State variables plotted over time for the "no control", the "reconstructed", and the optimal "social distancing control" scenarios in the state of Alabama using $\lambda_1 = 0.01$ and 4 distinct cost functions, $c_{1,j}(u_1)$, as defined in (2.8).

To illustrate the efficiency of various control strategies, we use real data for the SARS-CoV-2 Delta variant of the COVID-19 pandemic in Alabama and Maryland from July 9, 2021 to November 25, 2021 [78]. In this section, the "social distancing control" scenario is compared to what we call "reconstructed" and "no control" scenarios. The "reconstructed" (or "real-life") scenario is described by system (2.1), where pre-estimated parameter values for the state of Alabama are set at $N = 5,031,362$,

$\gamma_{u,r} = (1-0.005)/10$, $\gamma_{u,d} = 0.005/18.5$, $\gamma_{v,r} = (1-0.005/12.7)/10$, $\gamma_{v,d} = 0.005/18.5/12.7$, $\delta_r = 1/90$, $\delta_v = 0$, $\alpha = 0.8$, and $\mu = 0.0009143$ [76,77], while the time-dependent transmission rate, $\zeta(t)$, and case reporting rate, ψ, are reconstructed from CDC data [78] on daily new infections and deaths by regularized optimization algorithm. The reconstructed value of ψ is equal to 0.154 (95%CI:[0.149,0.159]) [77]. The initial values for (2.1) are $S_u(0) = 3,402,668/N$, $S_v(0) = 1,626,323/N$, $I_u(0) = 1584/N$, $I_v(0) = 787/N$, $R(0) = 0$, and $D(0) = 0$.

In the "reconstructed" or "real-life" scenario we assume that both social distancing and vaccination controls are present, but their implementation is not optimal and mimics real-life interventions put in place from 7/9/2021 to 11/25/2021. The hypothetical "no control" scenario is given by model (2.5), where neither social distancing nor vaccination control is applied. The hypothetical "social distancing control" scenario (3.1) represents the case where optimal social distancing control is implemented with no vaccination available (see Algorithm 1). The initial values for the state variables in these two cases are $S_u(0) = (3,402,668 + 1,626,323)/N$, $I_u(0) = (1584 + 787)/N$, $R(0) = 0$, and $D(0) = 0$. In (2.5) and (3.1), the constant transmission rate, β, is set to $0.416 = \max_{t \in [0,T]} \zeta(t)$ since $\zeta(t) = \beta(1 - \tilde{u}_1(t))$, where $\tilde{u}_1(t)$ is a "real-life" non-optimal social distancing control ($0 \le \tilde{u}_1(t) < 1$ for $t \in [0,T]$), as mentioned in Section 2 above.
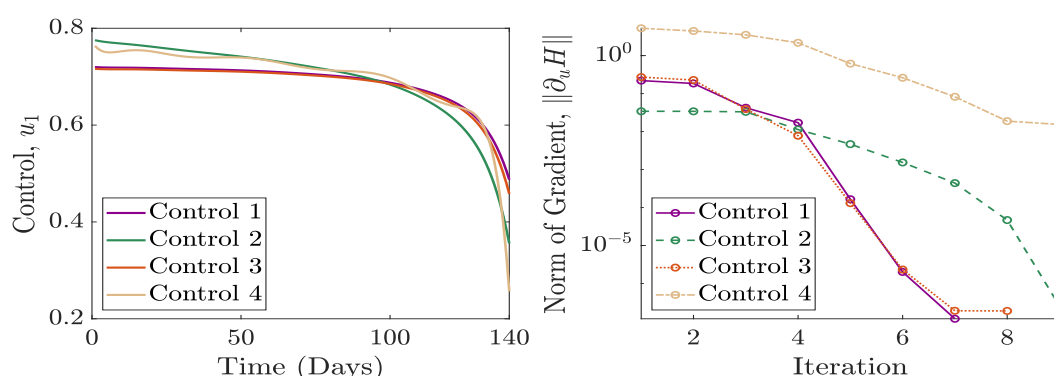

Figure 3. Optimal controls, $u_1(t)$, plotted over time for the "social distancing control" scenario in the state of Alabama (left) and the convergence rate for the norm of the gradient of the Hamiltonian with respect to u_1 (right) for $\lambda_1 = 0.01$ and 4 distinct cost functions, $c_{1,j}(u_1)$, as defined in (2.8).

Figure 2 shows that without any control measures in place, the daily number of infected people would be quite alarming until the strain runs its natural course. The hypothetical number of deceased individuals in the "no control" environment is dangerously high. On the other hand, with optimally enforced social distancing, even without vaccination, the daily number of infected and deceased humans is very low (though some cases appear to be delayed rather than prevented). The figure underscores the importance of social distancing in mitigating the impact of infectious disease outbreaks. The "reconstructed" curves in Figure 2 illustrate that the real-life control measures in the state of Alabama, which included both vaccination and social distancing, were very effective and saved many lives.

The first graph in Figure 3 demonstrates that optimal social distancing must be strictly enforced at the early ascending stage of a new wave in order to contain the virus. However, toward the end of the study period, the intensity of optimal control goes down due to its negative impact on the economy and overall quality of life. The figure shows that, for this particular value of $\lambda_1 = 0.01$, the control strategy

for all four cost functions (2.8) remains within the feasible set the entire time, without inequality constraints enforced. At the same time, according to the second graph in Figure 3, the control strategy associated with $c_{1,4}$ may not be a global minimum. One can see in Figure 1 that the cost of the 4th control is the highest among all costs considered. Therefore, superior results for the 4th control, shown in Figure 2, may be at the expense of the algorithm not sufficiently reducing the negative impact.
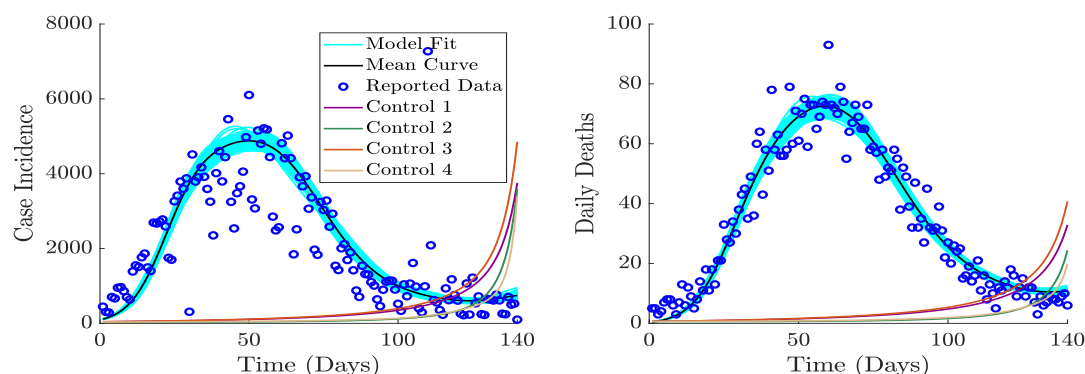

Figure 4. New incidence cases and daily deaths plotted over time for the hypothetical "social distancing control" scenario using $\lambda_1 = 0.01$ and 4 distinct cost functions, $c_{1,j}(u_1)$, as defined in (2.8) vs. real data for the state of Alabama from July 9, 2021 to November 25, 2021 [78].

Figure 4 compares the actual number of new daily infections and deaths in the state of Alabama from July 9, 2021 to November 25, 2021 [78], to new infections and deaths in the case of hypothetical optimally controlled social distancing (for the four cost functions (2.8)). It also illustrates the model fit with 100 bootstrapping iterations for uncertainty quantification [76, 77]. The figure supports our earlier observation that optimal implementation of social distancing prevents a considerable number of deaths. It illustrates that the daily number of newly infected people at the early stage of the cycle, where the optimal social distancing control is strictly enforced, is close to zero. However, new incidence cases and deaths increase toward the end of the study period, when the intensity of optimal control goes down. The surge of new infections and deaths in the last 40 days of the interval underlines the importance of a vaccination campaign for the prevention of cases. Optimal social distancing control is very powerful initially, but it is not sustainable for a long time.

Figures 5–7 represent the "no control", the "reconstructed", and the optimal "social distancing control" scenarios for the state of Maryland during the COVID-19 Delta variant from July 9, 2021 to November 25, 2021. By comparing Figures 2–4 to Figures 5–7, we can examine how regional differences, such as varying population density, healthcare infrastructure, and socioeconomic factors, influence the optimal control strategy [89, 90].

For the state of Maryland, the "reconstructed" scenario, described by system (2.1), illustrates the efficiency of real-life interventions. In Maryland model (2.1), some parameters are the same as in the case of Alabama and others are different (i.e., state-specific). The pre-estimated parameter values for the state of Maryland are $N = 6,173,205$, $\delta_r = 1/90$, $\gamma_{u,r} = (1 - 0.005)/10$, $\gamma_{u,d} = 0.005/18.5$, $\gamma_{v,r} = (1 - 0.005/12.7)/10$, $\gamma_{v,d} = 0.005/18.5/12.7$, $\delta_v = 0$, and $\mu = 0.0007286$ [76, 77]. The time-dependent transmission rate, $\zeta(t)$, and case reporting rate, ψ, are reconstructed from CDC data [78] on daily new infections and deaths by a regularized optimization algorithm. The reconstructed value of ψ for Maryland is equal to 0.182 (95%CI:[0.172,0.192]), see [77]. Pre-estimated initial values for

the coordinates of $\mathbf{x} := [S_u, S_v, I_u, I_v, R, D]^\top$ in (2.1) are $S_u(0) = 2,727,503/N$, $S_v(0) = 3,445,221/N$, $I_u(0) = 207/N$, $I_v(0) = 274/N$, $R(0) = 0$, and $D(0) = 0$.
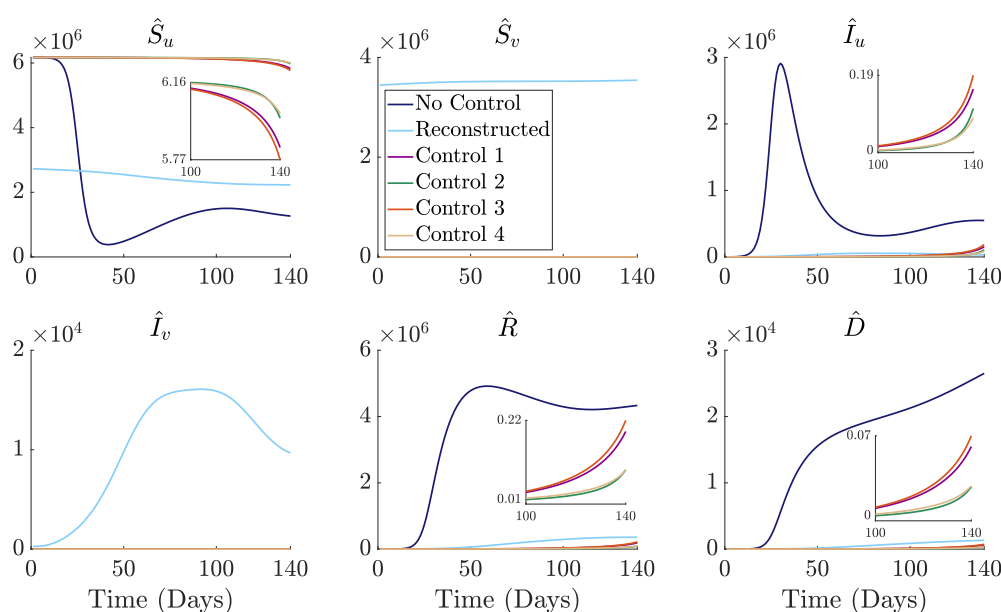

Figure 5. State variables plotted over time for the "no control", the "reconstructed", and the optimal "social distancing control" scenarios in the state of Maryland using $\lambda_1 = 0.01$ and 4 distinct cost functions, $c_{1,j}(u_1)$, as defined in (2.8).

As before, the hypothetical "no control" scenario is given by model (2.5) with no control applied, and the hypothetical "social distancing control" scenario (3.1) is the case where optimal social distancing control is employed with no vaccination available (see Algorithm 1). The initial values for systems (2.5) and (3.1) are $S_u(0) = (3,402,668 + 1,626,323)/N$, $I_u(0) = (1584 + 787)/N$, $R(0) = 0$, and $D(0) = 0$. In (2.5) and (3.1), the transmission rate, β, is set to $0.477 = \max_{t \in [0,T]} \zeta(t)$ since $\zeta(t) = \beta(1 - \tilde{u}_1(t))$, where $\tilde{u}_1(t)$ is a "real-life" non-optimal social distancing control ($0 \le \tilde{u}_1(t) < 1$ for $t \in [0, T]$).

As we look at Figures 2 and 5, it is important to keep in mind that at the start of the study period, in the state of Alabama, the percentage of fully vaccinated people was 33.2%, while in the state of Maryland it was 57%. At the end of the study period, these numbers were 46% and 67.2%, respectively. Hence it comes at no surprise that the daily number of infected people in Alabama (the "reconstructed" scenario) is higher than in Maryland. Figure 5, similar to Figure 2, underscores the importance of disease control in epidemic management. The figure shows a frightening number of infected and deceased people in a hypothetical uncontrolled environment. On the other hand, the "social distancing control" curves in Figure 5 prove the efficiency of this nonmedical form of disease prevention. The "reconstructed" scenario in Figure 5 convincingly shows that the real-life control measures in the state of Maryland worked well.

Figure 6 for Maryland is consistent with what was observed for the state of Alabama in Figure 3. To contain the spread of the virus, social distancing must be strictly enforced at the outset of a new strain. However, this form of control is not sustainable in the long run as the cost begins to take its toll. More than likely, the oscillating behavior of the social distancing control, $u_1(t)$, corresponding to the fourth

cost function, $c_{1,4}$, at the start of the interval is due to unavoidable instability of parameter estimation. As evident from the second graph in Figure 6, similar to the case of Alabama, $u_1(t)$ associated with $c_{1,4}$ may not be a global minimum. That is why it is so crucial to consider several cost functions to ensure reliable practical recommendations.
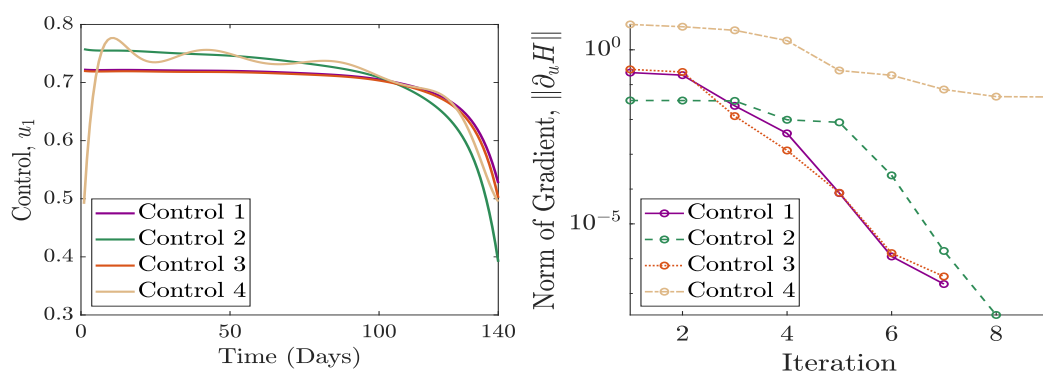

Figure 6. Optimal controls, $u_1(t)$, plotted over time for the "social distancing control" scenario in the state of Maryland (left) and the convergence rate for the norm of the gradient of the Hamiltonian with respect to u_1 (right) for $\lambda_1 = 0.01$ and 4 distinct cost functions, $c_{1,j}(u_1)$, as defined in (2.8).

Figure 7 illustrates that in the state of Maryland, with optimal social distancing control, the number of new cases and deaths would be significantly reduced during the first 100 days of the Delta strain. However, in the last 40 days, the trend is the exact opposite. Again, this highlights the importance of other control measures, such as vaccination and antiviral treatments, when social distancing inevitably becomes less aggressive over time.
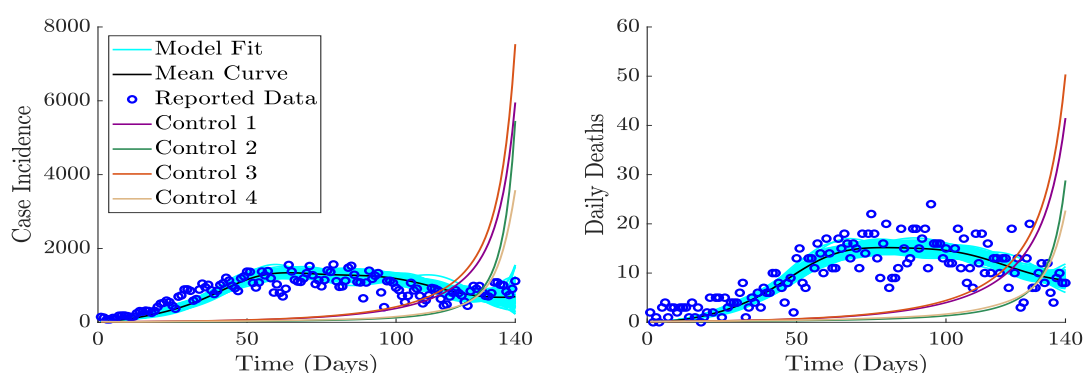

Figure 7. New incidence cases and daily deaths plotted over time for the hypothetical "social distancing control" scenario using $\lambda_1 = 0.01$ and 4 distinct cost functions, $c_{1,j}(u_1)$, as defined in (2.8) vs. real data for the state of Maryland from July 9, 2021 to November 25, 2021 [78].

4. Vaccination control

In this section, we define a mitigation scenario where only vaccination controls are employed, without any social distancing interventions. To accurately capture this scenario, we employ the $S_u S_v I_u I_v RD$

model with control $u_2(t) \in \mathcal{U}$ factored into the vaccination rate. The higher the value of the control, the stricter the vaccination measures, hopefully resulting in a lower number of cases and deaths. Without a social distancing control, the disease transmission rate, β, is assumed to be at its maximum value, defined as $\beta = \max_{t \in [0,T]} \zeta(t)$. Hence, the $S_u S_v I_u I_v R D$ model with vaccination control, $u_2(t)$, is as follows

$$
\begin{aligned}
\frac{dS_u}{dt} &= -\beta \frac{S_u(t)}{1 - D(t)}(I_u(t) + I_v(t)) - \nu u_2(t) S_u(t) + \delta_r R(t) + \delta_v S_v(t), \\
\frac{dS_v}{dt} &= -(1 - \alpha)\beta \frac{S_v(t)}{1 - D(t)}(I_u(t) + I_v(t)) + \nu u_2(t) S_u(t) - \delta_v S_v(t), \\
\frac{dI_u}{dt} &= \beta \frac{S_u(t)}{1 - D(t)}(I_u(t) + I_v(t)) - (\gamma_{u,r} + \gamma_{u,d})I_u(t), \\
\frac{dI_v}{dt} &= (1 - \alpha)\beta \frac{S_v(t)}{1 - D(t)}(I_u(t) + I_v(t)) - (\gamma_{v,r} + \gamma_{v,d})I_v(t), \\
\frac{dR}{dt} &= \gamma_{u,r} I_u(t) + \gamma_{v,r} I_v(t) - \delta_r R(t), \\
\frac{dD}{dt} &= \gamma_{u,d} I_u(t) + \gamma_{v,d} I_v(t).
\end{aligned}
\tag{4.1}
$$

In system (4.1), ν stands for the pre-estimated vaccination capacity, which is set to $1/7$ in our experiments implying that the entire population of the state can potentially be vaccinated in one week once vaccine becomes available for the general population. Of course, in reality, it is impossible to vaccinate everyone, which underlines the importance of the condition $\lim_{u \to 1^-} c_{i,j}(u) = \infty$, guaranteeing that the cost of control becomes prohibitive as u approaches the upper bound of the control range. Recall that for the cost functions $c_{i,j}(u)$, $i = 1, 2$, defined in (2.8), the above assumption is fulfilled when $j = 1, 3, 4$.
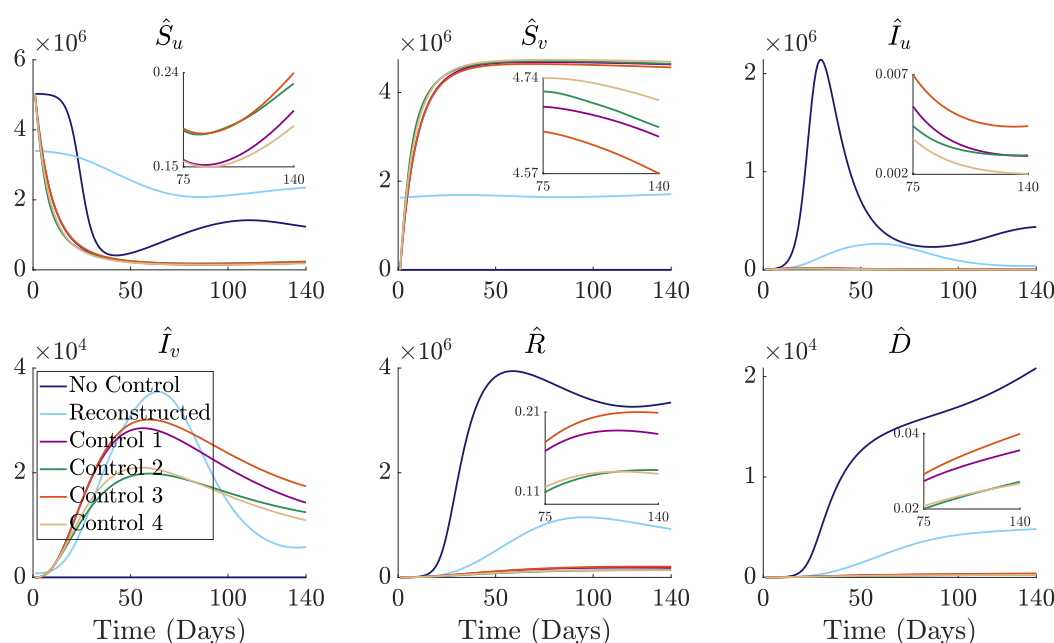

Figure 8. State variables plotted over time for the "no control", the "reconstructed", and the optimal "vaccine control" scenarios in the state of Alabama using $\lambda_2 = 0.01$ and 4 distinct cost functions, $c_{2,j}(u_2)$, as defined in (2.8).

In the "vaccine control" scenario, the normalized force of infection that one needs to minimize is equal to $\beta \frac{S_u(t)+(1-\alpha)S_v(t)}{1-D(t)}(I_u(t) + I_v(t))$, leading to the objective functional in the form:

$$J(\mathbf{x}, u_2) = \int_0^T \left\{ \beta \frac{S_u(t) + (1 - \alpha)S_v(t)}{1 - D(t)}(I_u(t) + I_v(t)) + \lambda_2 c_2(u_2(t)) \right\} dt$$

$$= (S_u + S_v)(0) - (S_u + S_v)(T) + \int_0^T \{\lambda_2 c_2(u_2(t)) + \delta_r R(t)\} dt, \tag{4.2}$$

$$\mathbf{x} = [S_u, S_v, I_u, I_v, R, D]^\top.$$

Taking into account Eqs (2.7), (4.1), and (4.2), we arrive at the following Hamiltonian, which is a critical component of the regularized numerical algorithm aimed at estimating the optimal vaccination strategy, $u_2(t)$, for the "vaccine control" problem:

$$H(\mathbf{x}, u_2, \mathbf{p}) = \lambda_2 c_2(u_2) + \delta_r R + p_1 \left[-\beta \frac{S_u}{1 - D}(I_u + I_v) - \nu u_2 S_u + \delta_r R + \delta_v S_v \right]$$

$$+ p_2 \left[-(1 - \alpha)\beta \frac{S_v}{1 - D}(I_u + I_v) + \nu u_2 S_u - \delta_v S_v \right] + p_3 \left[\beta \frac{S_u}{1 - D}(I_u + I_v) \right.$$

$$\left. - (\gamma_{u,r} + \gamma_{u,d})I_u \right] + p_4 \left[(1 - \alpha)\beta \frac{S_v}{1 - D}(I_u + I_v) - (\gamma_{v,r} + \gamma_{v,d})I_v \right]$$

$$+ p_5 \left[\gamma_{u,r}I_u + \gamma_{v,r}I_v - \delta_r R \right] + p_6 \left[\gamma_{u,d}I_u + \gamma_{v,d}I_v \right], \tag{4.3}$$

where $\mathbf{p} := [p_1, p_2, p_3, p_4, p_5, p_6]^\top$. From Pontryagin's Minimum Principle [33,83], one concludes that $u_2 = \arg\min_{v \in \mathcal{U}} H(\mathbf{x}, v, \mathbf{p})$, subject to state system (4.1) and costate system (2.6):

$$\frac{dp_1}{dt} = \frac{\beta[I_u(t) + I_v(t)]}{1 - D(t)}[p_1(t) - p_3(t)] + \nu u_2(t)[p_1(t) - p_2(t)],$$

$$\frac{dp_2}{dt} = \frac{\beta(1 - \alpha)[I_u(t) + I_v(t)]}{1 - D(t)}[p_2(t) - p_4(t)] + \delta_v[p_2(t) - p_1(t)],$$

$$\frac{dp_3}{dt} = \frac{\beta S_u(t)}{1 - D(t)}[p_1(t) - p_3(t)] + (1 - \alpha)\frac{\beta S_v(t)}{1 - D(t)}[p_2(t) - p_4(t)] + \gamma_{u,r}[p_3(t) - p_5(t)]$$

$$+ \gamma_{u,d}[p_3(t) - p_6(t)],$$

$$\frac{dp_4}{dt} = \frac{\beta S_u(t)}{1 - D(t)}[p_1(t) - p_3(t)] + (1 - \alpha)\frac{\beta S_v(t)}{1 - D(t)}[p_2(t) - p_4(t)] + \gamma_{v,r}[p_4(t) - p_5(t)] \tag{4.4}$$

$$+ \gamma_{v,d}[p_4(t) - p_6(t)],$$

$$\frac{dp_5}{dt} = \delta_r[p_5(t) - p_1(t) - 1],$$

$$\frac{dp_6}{dt} = \frac{\beta S_u(t)[I_u(t) + I_v(t)]}{(1 - D(t))^2}[p_1(t) - p_3(t)] + (1 - \alpha)\frac{\beta S_v(t)[I_u(t) + I_v(t)]}{(1 - D(t))^2}[p_2(t) - p_4(t)],$$

and $\mathbf{p}(T) = [-1, -1, 0, 0, 0, 0]^\top$. Thus, for the "vaccine control" scenario, one obtains the following 2nd-order algorithm for nonlinear constrained minimization:

Algorithm 2 Numerical method for solving the vaccination optimal control problem

Require: Cost function $c_{2,j}(u_2)$, weight λ_2, finite dimensional approximation $u_2[\theta]$, initial guess θ.
Ensure: Optimal control $u_2[\theta]$ with estimated θ.
   repeat
      Solve (4.1) for **x** forward in time.
      Solve (4.4) for **p** backward in time.
      $\theta \leftarrow \theta - \varrho(J^{\top}(\theta)J(\theta) + \omega_k I)^{-1}J^{\top}(\theta)F(\theta)$.
   until converged.

In Algorithm 2, $F(\theta)$ is a discrete analog of the partial derivative of the Hamiltonian, $H(\mathbf{x}, u_2, \mathbf{p})$, with respect to u_2, $J(\theta)$ is the Jacobian of $F(\theta)$, I is the identity matrix in the solution space, ϱ is the step size, and ω_k is the regularization sequence. The derivative of $H(\mathbf{x}, u_2, \mathbf{p})$ with respect to u_2 exists, since $c_{2,j}(u)$, $j = 1, 2, 3, 4$, are twice continuously differentiable by our assumption. As in the previous section, in all our experiments, shifted Legendre polynomials were used to project the control function, $u_2(t)$, onto a finite dimensional subspace with θ being a vector of expansion coefficients. MATLAB's built-in function "ode15s" was employed to solve both ODE systems, (4.1) and (4.4), while "lsqnonlin" implemented the Levenberg-Marquardt optimization procedure.
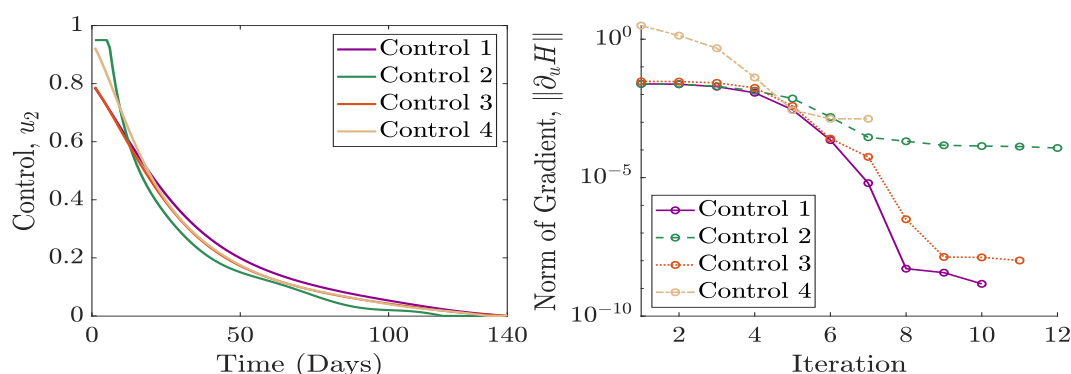

Figure 9. Optimal controls, $u_2(t)$, plotted over time for the "vaccine control" scenario in the state of Alabama (left) and the convergence rate for the norm of the gradient of the Hamiltonian with respect to u_2 (right) for $\lambda_2 = 0.01$ and 4 distinct cost functions, $c_{2,j}(u_2)$, as defined in (2.8).

In what follows, we present numerical results comparing the "no control", the "reconstructed", and the "vaccine control" scenarios for managing the COVID-19 Delta variant in the states of Alabama and Maryland. The "reconstructed" (or "real-life") scenario is described by system (2.1), where pre-estimated parameter values for Alabama and Maryland are the same as in Section 3. In the "reconstructed" or "real-life" scenario, we assume that both social distancing and vaccination controls are present, but their implementation is not optimal and mimics real-life interventions put in place from 7/9/2021 to 11/25/2021. The hypothetical "no control" scenario is given by model (2.5), where neither social distancing nor vaccination control is applied. The hypothetical "vaccine control" scenario (4.1) represents the case where optimal vaccination control is implemented in the absence of social distancing measures (see Algorithm 2).

Figure 8 illustrates the disease progression in Alabama from July 9, 2021 to November 25, 2021,

highlighting the significant impact of vaccination control throughout the study period. The results suggest that the optimal vaccination strategy involves quickly vaccinating a large portion of the population - over 90%. Numerical experiments demonstrate that vaccinating people early on leads to a substantial decline in the daily number of infected individuals. This translates into a considerable reduction in COVID-related deaths during the same period of time, which further confirms the benefits of early vaccination.
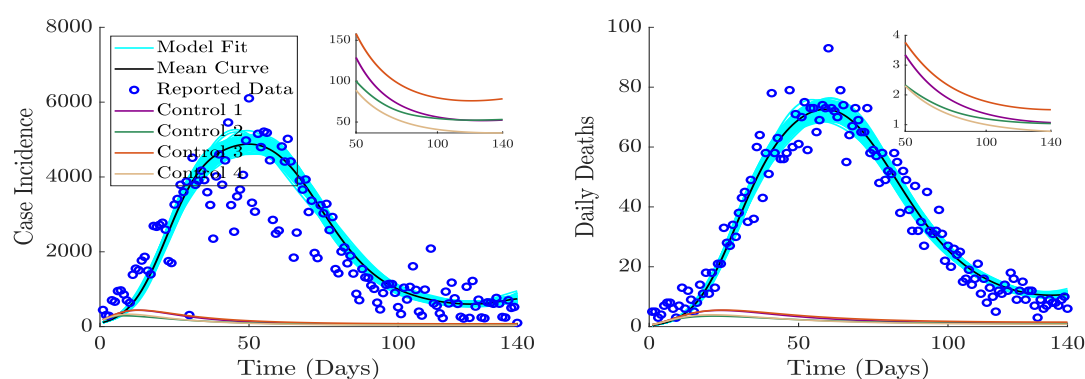

Figure 10. New incidence cases and daily deaths plotted over time for the hypothetical "vaccine control" scenario using $\lambda_2 = 0.01$ and 4 distinct cost functions, $c_{2,j}(u_2)$, as defined in (2.8) vs. real data for the state of Alabama from July 9, 2021 to November 25, 2021 [78].

Figure 11. State variables plotted over time for the "no control", the "reconstructed", and the optimal "vaccine control" scenarios in the state of Maryland using $\lambda_2 = 0.01$ and 4 distinct cost functions, $c_{2,j}(u_2)$, as defined in (2.8).

Figure 8 also underscores that the "real-life" preventive measures, including social distancing and vaccination, were very beneficial. At the same time, vaccinating a higher percentage of people before

or right after the start of the Delta strain could have prevented even more infections and further depleted the number of deaths. Figure 9 reinforces the message that optimal vaccine control must be applied very early and nearly to its full capacity. Over time, the intensity of vaccine control, understandably, needs to go down due to the lasting benefits of vaccination.

Figure 12. Optimal controls, $u_2(t)$, plotted over time for the "vaccine control" scenario in the state of Maryland (left) and the convergence rate for the norm of the gradient of the Hamiltonian with respect to u_2 (right) for $\lambda_2 = 0.01$ and 4 distinct cost functions, $c_{2,j}(u_2)$, as defined in (2.8).

All control strategies shown in Figure 9 adhere to feasible constraints (without these constraints being imposed in the algorithm) for all values of $t \in [0, T]$, with the exception of $u_2(t)$, corresponding to the cost function $c_{2,2}(u) = u^2$, for which both upper and lower bounds need to be enforced. Thus, Figure 9, once again, demonstrates the importance of the condition $\lim_{u \to 1^-} c_{i,j}(u) = \infty$. The second graph in Figure 9 shows that control strategies associated with $c_{1,2}$ and $c_{1,4}$ are not likely to be global minima. Similar to the case of "social distancing control", advantages of the 4th control, seen in Figure 8, may be due to insufficient cost reduction.

Figure 13. New incidence cases and daily deaths plotted over time for the hypothetical "vaccine control" scenario using $\lambda_2 = 0.01$ and 4 distinct cost functions, $c_{2,j}(u_2)$, as defined in (2.8) vs. real data for the state of Maryland from July 9, 2021 to November 25, 2021 [78].
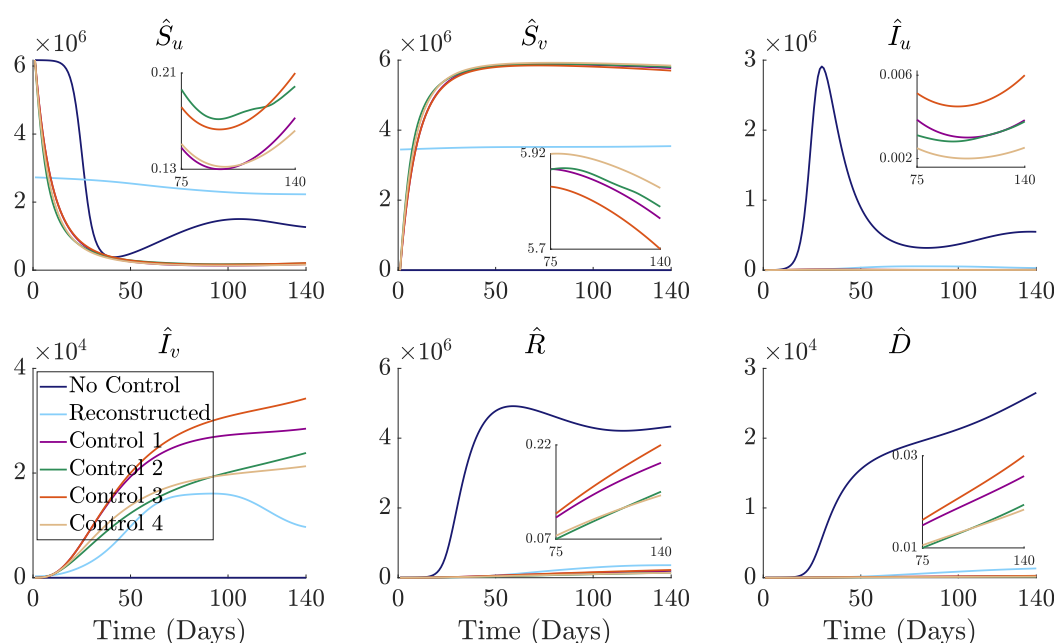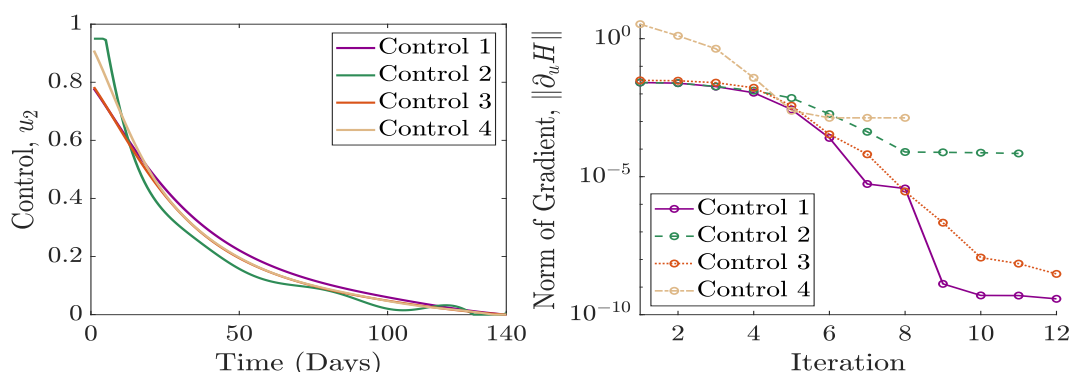
Examining Figures 4 and 10, one can clearly see a major difference in disease dynamics for "social distancing control" and "vaccine control" scenarios. In the case of optimal "social distancing control"

(Figure 4), new COVID cases and deaths are surging toward the end of the study period calling for immediate further interventions. However, the optimal "vaccine control" strategy (Figure 10) reliably "flattens the curve" for the entire interval of time, demonstrating a lasting positive impact of prompt early vaccination.

Figures 11 and 12 make essentially the same case for the optimal "vaccine control" scenario as Figures 8 and 9, that is, for the best outcome, vaccination needs to be done early and it has to include as many people as possible. In terms of the algorithm, Figures 9 and 12 reiterate that condition $\lim_{u \to 1^-} c_{i,j}(u) = \infty$ is critical. For solution $u_2(t)$, corresponding to the cost function $c_{2,2}(u) = u^2$, to generate a practically relevant control strategy, the bounds of the feasible set need to be enforced in the course of optimization. Once again, the second graph in Figure 12 illustrates that control strategies associated with $c_{1,2}$ and $c_{1,4}$ are not likely to be global minima.

The long-term efficiency of the optimal vaccination control is even more pronounced if one compares Figures 7 and 13 for the state of Maryland. In Figure 7, showing the hypothetical social distancing intervention, one can observe a catastrophic increase in daily new cases and deaths in the last 40 days of the study interval. At the same time, for the "reconstructed" scenario in Maryland, in the last 40 days, the epidemic is safely contained. Figure 13, contrasting the optimal "vaccine control" and the "reconstructed" real-life progression, makes a convincing case for the optimal vaccination strategy, which is clearly superior to the "reconstructed" and "social distancing" scenarios by a very large margin.

5. Both controls concurrently

In this section, we explore a general scenario where both social distancing and vaccination controls are implemented concurrently. To model this optimal control problem, we employ the $S_u S_v I_u I_v RD$ system (2.3) introduced in Section 2. In system (2.3), a control $u_1(t)$ is factored into the transmission rate to account for social distancing and a control $u_2(t)$ is factored into the vaccination rate to account for movement of individuals between susceptible unvaccinated and vaccinated compartments. To balance the pros and cons of optimal controls, $u_1(t)$ and $u_2(t)$, we minimize the objective functional (2.4) subject to system (2.3). As it follows from (2.7), (2.3), and (2.4), the Hamiltonian for the "both controls concurrently" scenario is given by the equation:

$$
\begin{aligned}
H(\mathbf{x}, \mathbf{u}, \mathbf{p}) = {} & \lambda_1 c_1(u_1) + \lambda_2 c_2(u_2) + \delta_r R \\
& + p_1 \left[-\beta(1 - u_1)\frac{S_u}{1 - D}(I_u + I_v) - \nu u_2 S_u + \delta_r R + \delta_v S_v \right] \\
& + p_2(t) \left[-(1 - \alpha)\beta(1 - u_1)\frac{S_v}{1 - D(t)}(I_u + I_v) + \nu u_2 S_u - \delta_v S_v \right] \\
& + p_3(t) \left[\beta(1 - u_1)\frac{S_u}{1 - D}(I_u + I_v) - (\gamma_{u,r} + \gamma_{u,d})I_u \right] \\
& + p_4(t) \left[(1 - \alpha)\beta(1 - u_1)\frac{S_v}{1 - D}[I_u + I_v] - (\gamma_{v,r} + \gamma_{v,d})I_v \right] \\
& + p_5(t) \left[\gamma_{u,r}I_u + \gamma_{v,r}I_v - \delta_r R \right] + p_6(t) \left[\gamma_{u,d}I_u + \gamma_{v,d}I_v \right].
\end{aligned}
\tag{5.1}
$$

Taking into account Pontryagin's Minimum Principle [33, 83], we recall that the costate system of equations, corresponding to our controlled biological model (2.3), satisfies

$$
\dot{\mathbf{p}}(t) = -\partial_{\mathbf{x}} H(\mathbf{x}, \mathbf{u}, \mathbf{p})^{\top} \big|_{\mathbf{x}(t), \mathbf{u}(t), \mathbf{p}(t)}, \quad \mathbf{p}(T) = \partial_{\mathbf{x}} h(\mathbf{x})^{\top} \big|_{\mathbf{x}(T)}.
$$

This gives rise to the following ODE system, $\mathbf{p}(T) = [-1, -1, 0, 0, 0, 0]$:

$$\frac{dp_1}{dt} = \frac{\beta(1 - u_1(t))[I_u(t) + I_v(t)]}{1 - D(t)}[p_1(t) - p_3(t)] + \nu u_2(t)[p_1(t) - p_2(t)],$$

$$\frac{dp_2}{dt} = \frac{\beta(1 - \alpha)(1 - u_1(t))[I_u(t) + I_v(t)]}{1 - D(t)}[p_2(t) - p_4(t)] + \delta_v[p_2(t) - p_1(t)],$$

$$\frac{dp_3}{dt} = \frac{\beta S_u(t)(1 - u_1(t))}{1 - D(t)}[p_1(t) - p_3(t)] + (1 - \alpha)\frac{\beta S_v(t)(1 - u_1(t))}{1 - D(t)}[p_2(t) - p_4(t)]$$
$$+ \gamma_{u,r}[p_3(t) - p_5(t)] + \gamma_{u,d}[p_3(t) - p_6(t)],$$

$$\frac{dp_4}{dt} = \frac{\beta S_u(t)(1 - u_1(t))}{1 - D(t)}[p_1(t) - p_3(t)] + (1 - \alpha)\frac{\beta S_v(t)(1 - u_1(t))}{1 - D(t)}[p_2(t) - p_4(t)] \qquad (5.2)$$
$$+ \gamma_{v,r}[p_4(t) - p_5(t)] + \gamma_{v,d}[p_4(t) - p_6(t)],$$

$$\frac{dp_5}{dt} = \delta_r[p_5(t) - p_1(t) - 1],$$

$$\frac{dp_6}{dt} = \frac{\beta S_u(t)(1 - u_1(t))[I_u(t) + I_v(t)]}{(1 - D(t))^2}[p_1(t) - p_3(t)]$$
$$+ (1 - \alpha)\frac{\beta S_v(t)(1 - u_1(t))[I_u(t) + I_v(t)]}{(1 - D(t))^2}[p_2(t) - p_4(t)].$$

To minimize (5.1) subject to Eqs (2.3) and (5.2), we propose the Levenberg-Marquardt optimization algorithm:

Algorithm 3 Numerical method for solving the optimal control problem with social distancing and vaccination controls implemented concurrently

---

Require: Cost function $\mathbf{c}(\mathbf{u})$, weight λ, finite dimensional approximation $\mathbf{u}[\theta]$, initial guess θ.
Ensure: Optimal control $\mathbf{u}[\theta]$ with estimated θ.
  repeat
    Solve (2.3) for $\mathbf{x}$ forward in time.
    Solve (5.2) for $\mathbf{p}$ backward in time.
    $\theta \leftarrow \theta - \varrho(J^\top(\theta)J(\theta) + \omega_k I)^{-1} J^\top(\theta)F(\theta)$.
  until converged.

In Algorithm 3, $F(\theta)$ is a discrete analog of $\partial_\mathbf{u}H(\mathbf{x}, \mathbf{u}, \mathbf{p})$, $J(\theta)$ is the Jacobian of $F(\theta)$, I is the identity matrix in the solution space, ϱ is the step size, and ω_k is the regularization sequence. We point out that $\partial_\mathbf{u}H(\mathbf{x}, \mathbf{u}, \mathbf{p})$ exists, since $c_{i,j}(u)$, $i = 1, 2$, $j = 1, 2, 3, 4$, are twice continuously differentiable by our assumption. In all our experiments, shifted Legendre polynomials were used to project the control function, $\mathbf{u}$, onto a finite dimensional subspace with θ being a vector of expansion coefficients. Matlab built-in function "ode15s" was employed to solve both ODE systems, (2.3) and (5.2), while "lsqnonlin" implemented the trust-region optimization procedure.

To illustrate the efficiency of the "both controls concurrently" intervention strategy, we present numerical experiments with real data for the SARS-CoV-2 Delta variant of the COVID-19 pandemic in Alabama and Maryland from July 9, 2021 to November 25, 2021 [78]. In this section, the "both controls concurrently", "reconstructed", and "no control" scenarios are compared. In the "reconstructed" or "real-life" scenario (2.1) we assume that both social distancing and vaccination controls are present,

but their implementation is not optimal and mimics real-life interventions put in place from 7/9/2021 to 11/25/2021. The hypothetical "both controls concurrently" scenario (2.3), represents the case where social distancing and vaccination controls are optimized in the sense of the objective functional (2.4).
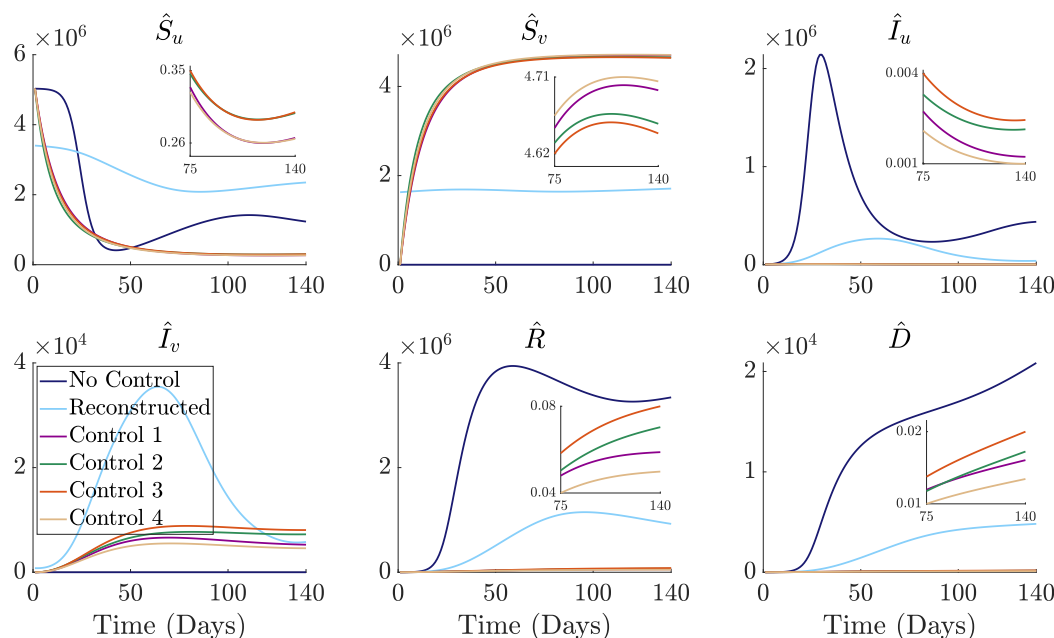

Figure 14. State variables plotted over time for the "no control", the "reconstructed", and the optimal "both controls concurrently" scenarios in the state of Alabama using $\lambda_1 = \lambda_2 = 0.01$, and $c_{1,j}(u_1) = c_{2,j}(u_2)$, $j = 1, 2, 3, 4$, as defined in (2.8).

Figure 15. Optimal controls, $\mathbf{u}(t)$, plotted over time for the "both controls concurrently" scenario in Alabama (left) and the convergence rate for the norm of the gradient of the Hamiltonian with respect to $\mathbf{u}$ (right) for $\lambda_1 = \lambda_2 = 0.01$ and $c_{1,j}(u_1) = c_{2,j}(u_2)$, $j = 1, 2, 3, 4$, as defined in (2.8).

The pre-estimated parameters for Alabama in these two cases are $N = 5,031,362$, $\delta_r = 1/90$, $\gamma_{u,r} = (1-0.005)/10$, $\gamma_{u,d} = 0.005/18.5$, $\gamma_{v,r} = (1-0.005/12.7)/10$, $\gamma_{v,d} = 0.005/18.5/12.7$, $\delta_v = 0$, and $\alpha = 0.8$ [76, 77], while the time-dependent transmission rate, $\zeta(t)$, for (2.1) and case reporting rate, ψ, are reconstructed from CDC data [78] on daily new infections and deaths by a regularized optimization

algorithm. The reconstructed value of ψ is equal to 0.154 (95%CI:[0.149,0.159]) [77]. In (2.1), for the state of Alabama, the average vaccination rate, μ, is equal to 0.0009143, while the vaccination capacity, ν, in (2.3) is set to 1/7. The initial values for systems (2.3) and (2.1) are $S_u(0) = 3,402,668/N$, $S_v(0) = 1,626,323/N$, $I_u(0) = 1584/N$, $I_v(0) = 787/N$, $R(0) = 0$, and $D(0) = 0$.

The hypothetical "no control" scenario is given by model (2.5), where neither social distancing nor vaccination control is applied. The initial values in this case are $S_u(0) = (3,402,668 + 1,626,323)/N$, $I_u(0) = (1584 + 787)/N$, $R(0) = 0$, $D(0) = 0$. In (2.5) and (3.1), the constant transmission rate, β, is set to $0.416 = \max_{t\in[0,T]} \zeta(t)$ since $\zeta(t) = \beta(1 - \tilde{u}_1(t))$, where $\tilde{u}_1(t)$ is a "real-life" non-optimal social distancing control ($0 \le \tilde{u}_1(t) < 1$ for $t \in [0,T]$), as mentioned in Section 2 above.

Figure 16. New incidence cases and daily deaths plotted over time for the hypothetical "both controls concurrently" scenario using $\lambda_1 = \lambda_2 = 0.01$ and $c_{1,j}(u_1) = c_{2,j}(u_2)$, $j = 1,2,3,4$, as defined in (2.8) vs. real data for the state of Alabama from July 9, 2021 to November 25, 2021 [78].
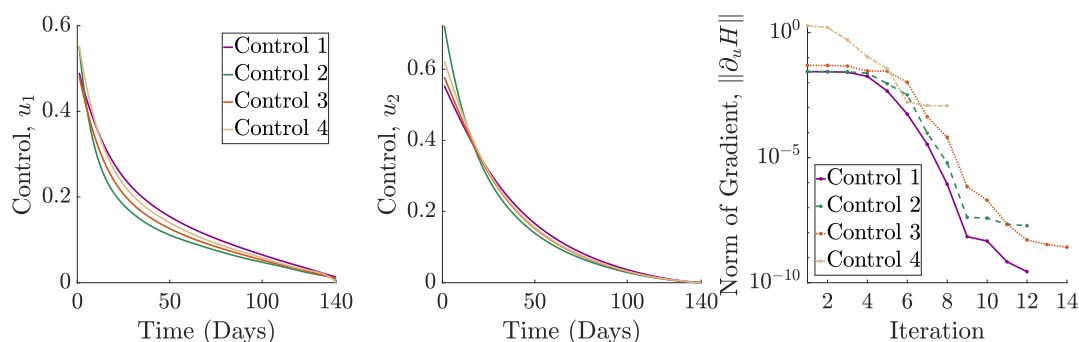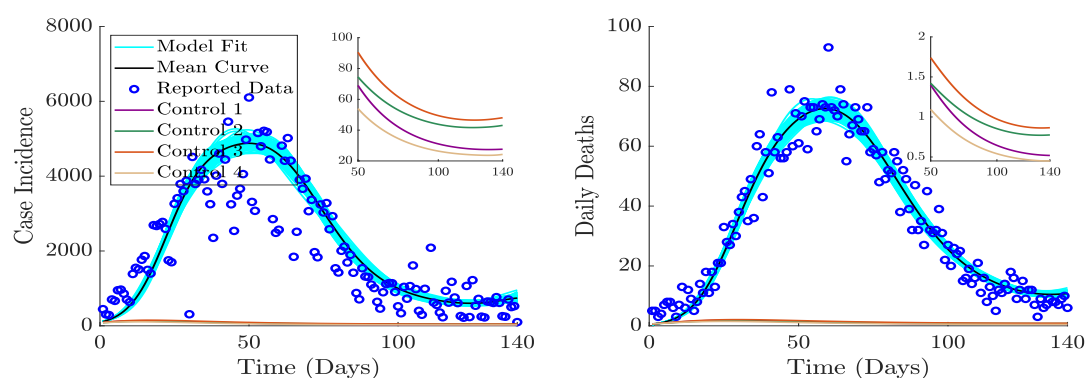
Figure 14, showing disease progression in the state of Alabama, illustrates superior efficiency of the hypothetical optimal "both controls concurrently" strategy. A comparison of Figures 9 and 15 demonstrates that in the presence of social distancing mitigation measures, the vaccination campaign at the start of the strain can be less rigorous. Figures 10 and 16 underscore that, in combination, optimal social distancing and vaccination controls achieve better results than "vaccine control" without either control being enforced too aggressively. Figures 9 and 15 show that after the initial push, which keeps the epidemic reliably contained, both social distancing and vaccination controls can be scaled down very quickly saving considerable resources. This highlights the importance of simultaneously applying multiple control strategies to combat disease outbreaks and to minimize their negative consequences.

The state-specific parameters for the Maryland "reconstructed" scenario, described by system (2.1), are $N = 6,173,205$ and $\mu = 0.0007286$ [76,77]. The time-dependent transmission rate, $\zeta(t)$, and case reporting rate, ψ, are estimated from CDC data [78] on daily new infections and deaths by a regularized optimization algorithm. The reconstructed value of ψ for Maryland is equal to 0.182 (95%CI:[0.172,0.192]). In ODE systems (2.1) and (2.3), the initial values for the coordinates of $\mathbf{x} := [S_u, S_v, I_u, I_v, R, D]^\top$ in the state of Maryland are $S_u(0) = 2,727,503/N$, $S_v(0) = 3,445,221/N$, $I_u(0) = 207/N$, $I_v(0) = 274/N$, $R(0) = 0$, and $D(0) = 0$. [77]. As before, the hypothetical "no control" scenario is given by model (2.5) with no control applied. The initial values for the variables of $\mathbf{x} := [S_u, I_u, R, D]^\top$ are $S_u(0) = (3,402,668 + 1,626,323)/N$, $I_u(0) = (1584 + 787)/N$, $R(0) = 0$, and $D(0) = 0$. In (2.3) and (2.5), the constant transmission rate, β, is set to $0.477 = \max_{t\in[0,T]} \zeta(t)$.

Figures 17–19 emphasize that applying social distancing and vaccine controls in combination is the most powerful way to contain the outbreak. By comparing "both controls concurrently" scenarios for Alabama and Maryland in Figures 15 and 18, respectively, one can notice that in both states, more emphasis is placed on vaccination than on social distancing. However, the two controls quickly decrease at a near-exponential rate due to a sustainable positive effect of vaccination.

Figure 17. State variables plotted over time for the "no control", the "reconstructed", and the optimal "both controls concurrently" scenarios in the state of Maryland using $\lambda_1 = \lambda_2 = 0.01$, and $c_{1,j}(u_1) = c_{2,j}(u_2)$, $j = 1, 2, 3, 4$, as defined in (2.8).

Figure 18. Optimal controls, $\mathbf{u}(t)$, plotted over time for the "both controls concurrently" scenario in Maryland (left) and the convergence rate for the norm of the gradient of the Hamiltonian with respect to $\mathbf{u}$ (right) for $\lambda_1 = \lambda_2 = 0.01$ and $c_{1,j}(u_1) = c_{2,j}(u_2)$, $j = 1, 2, 3, 4$, as defined in (2.8).

As in all previous cases, the 4th control may not be a global minimum of the Hamiltonian as suggested by the second graphs in Figures 15 and 18. The first three controls, including the one that

corresponds to $c_{1,2}(u) = c_{2,2}(u) = u^2$, appear to be global minima, and no bounds need to be enforced by the optimization algorithm.

Figure 19. New incidence cases and daily deaths plotted over time for the hypothetical "both controls concurrently" scenario using $\lambda_1 = \lambda_2 = 0.01$ and $c_{1,j}(u_1) = c_{2,j}(u_2)$, $j = 1, 2, 3, 4$, as defined in (2.8) vs. real data for Maryland from July 9, 2021 to November 25, 2021 [78].
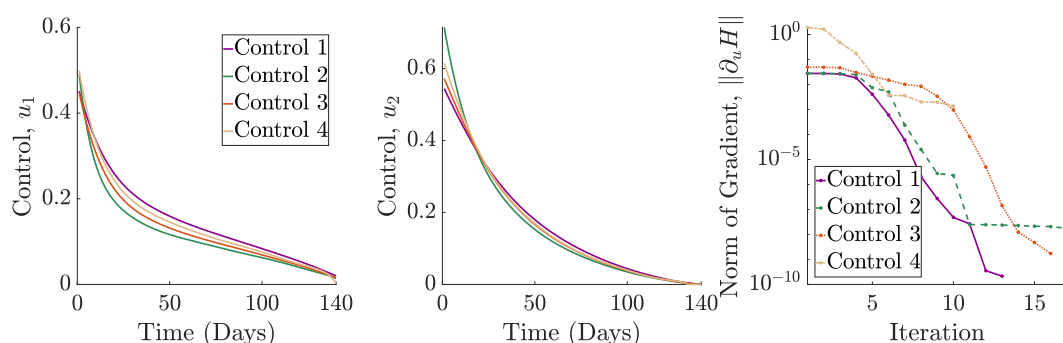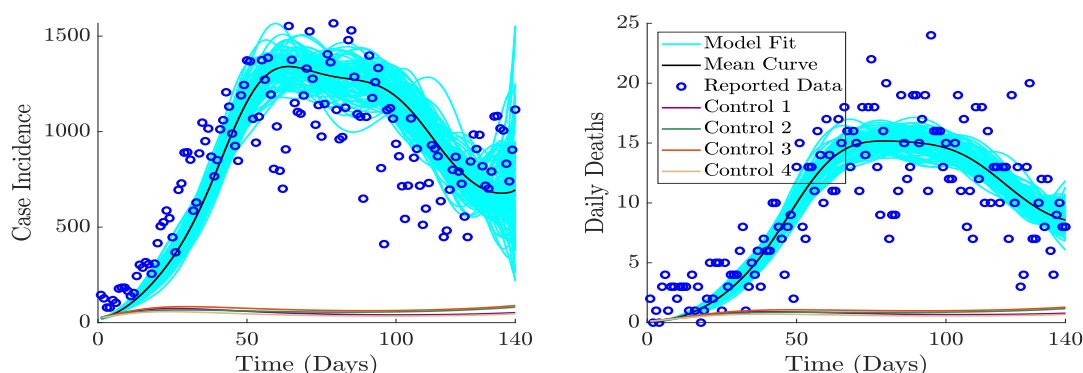
6. Conclusions and future plans

Control and prevention strategies are indispensable tools for managing the spread of infectious diseases. This paper examines biological models for the post-vaccination stage of a viral outbreak that integrate two important mitigation tools: social distancing, aimed at reducing the disease transmission rate, and vaccination, which boosts the immune system. Five different scenarios of epidemic progression are considered: (i) the "no control" scenario, reflecting the natural evolution of a disease without any safety measures in place, (ii) the "reconstructed" scenario, representing real-world data and interventions, (iii) the "social distancing control" scenario covering a broad set of behavioral changes, (iv) the "vaccine control" scenario demonstrating the impact of vaccination on epidemic spread, and (v) the "both controls concurrently" scenario incorporating social distancing and vaccine controls simultaneously. By investigating these scenarios, we provide a comprehensive analysis of various intervention strategies, offering valuable insights into disease dynamics.

Figures A1–A8 in the Appendix section compare the evolution of state variables, $\hat{S}_u$, $\hat{S}_v$, $\hat{I}_u$, $\hat{I}_v$, $\hat{R}$, $\hat{D}$, for "social distancing control", "vaccine control", and "both controls concurrently" mitigation frameworks in Alabama and Maryland versus the corresponding state variables reconstructed from real data from July 9, 2021 to November 25, 2021 [78]. Tables A1–A8 in the Appendix compare the daily number of infected people, $\hat{I}_u + \hat{I}_v$, for the same controls and over the same period of time. The main findings of our numerical study are as follows:

- Strict social distancing at the early ascending stage of a new virus wave has immediate positive impact and saves a lot of lives. Early on, optimal social distancing is more efficient than optimal vaccination. However, social distancing is not sustainable in the long run since the cost of this extreme control measure eventually takes its toll. Thus, the intensity of social distancing control begins to slow down after about three months. When social distancing policies are relaxed, new incidence cases and daily new deaths surge. This hypothetical surge is particularly noticeable in Maryland as compared to real data (see Figure 7).

- The positive impact of optimal vaccination is not immediate. But once vaccination takes effect, it works exceptionally well. Experiments show that vaccine control can be safely scaled down after the initial rapid action without any risk of cases increasing or more people dying toward the end of the study window.

- Given the unique individual properties of social distancing and vaccination, the best outcome is achieved when the two controls are applied concurrently. Together, these interventions complement each other. They quickly "flatten the curve" and prevent infections from rebounding in the last 40 days. After prompt early response, both controls quickly decrease at a near-exponential rate due to the sustainable positive effect of vaccination. In all scenarios considered, the results obtained with $c_{i,4}(u) = -u \ln(1 - u)$ should be taken with a grain of salt, since the corresponding control function may not be a global minimum of the Hamiltonian.

- To reconstruct unknown parameters for the optimal control problem, quantification of uncertainty related to noise in the reported data was carried out by refitting model (2.1) to $M = 100$ additional data sets assuming a Poisson error structure. The resulting M best-fit parameter sets were used to find the 95% confidence intervals and to estimate the mean values [76, 77]. In our future work, we plan to replace system (2.1) with a stochastic compartmental model governed by Wiener processes, which takes into account the uncertainty of the disease transmission, incubation period, and variability of detection.

Use of AI tools declaration

The authors declare they have not used Artificial Intelligence (AI) tools in the creation of this article.

Acknowledgments

Conflict of interest

The authors declare there is no conflict of interest.

References

1. W. Wu, Y. Yang, G. Sun, Recent insights into antibiotic resistance in Helicobacter pylori eradication, *Gastroenterol. Res. Pract.*, **2012** (2012), 723183. https://doi.org/10.1155/2012/723183

2. M. Wierup, The control of microbial diseases in animals: alternatives to the use of antibiotics, *Int. J. Antimicrob. Agents*, **14** (2000), 315–319. https://doi.org/10.1016/S0924-8579(00)00143-6

3. R. C. Waite, Y. Velleman, G. Woods, A. Chitty, M. C. Freeman, Integration of water, sanitation and hygiene for the control of neglected tropical diseases: a review of progress and the way forward, *Int. Health*, **8** (2015), i22–i27. https://doi.org/10.1093/inthealth/ihw003

4. A. Hinman, Eradication of vaccine-preventable diseases, *Annu. Rev. Public Health*, **20** (1999), 211–229. https://doi.org/10.1146/annurev.publhealth.20.1.211

5. S. Barrett, Eradication versus control: the economics of global infectious disease policies, *Bull. World Health Organ.*, **82** (2004), 683–688.

6. P. Aaby, C. S. Benn, Stopping live vaccines after disease eradication may increase mortality, *Vaccine*, **38** (2020), 10–14. https://doi.org/10.1016/j.vaccine.2019.10.034

7. N. L. Stepan, *Eradication: Ridding the World of Diseases Forever?*, Reaktion Books, 2013.

8. W. R. Dowdle, The principles of disease elimination and eradication, *Bull. World Health Organ.*, **76** (1998), 22–25.

9. B. Beović, The issue of antimicrobial resistance in human medicine, *Int. J. Food Microbiol.*, **112** (2006), 280–287. https://doi.org/10.1016/j.ijfoodmicro.2006.05.001

10. D. S. Schneider, J. S. Ayres, Two ways to survive infection: what resistance and tolerance can teach us about treating infectious diseases, *Nat. Rev. Immunol.*, **8** (2008), 889–895. https://doi.org/10.1038/nri2393

11. B. Spellberg, R. Guidos, D. Gilbert, J. Bradley, H. W. Boucher, W. M. Scheld, et al., The epidemic of antibiotic-resistant infections: a call to action for the medical community from the Infectious Diseases Society of America, *Clin. Infect. Dis.*, **46** (2008), 155–164. https://doi.org/10.1086/524891

12. G. J. Armelagos, P. J. Brown, B. Turner, Evolutionary, historical and political economic perspectives on health and disease, *Social Sci. Med.*, **61** (2005), 755–765. https://doi.org/10.1016/j.socscimed.2004.08.066

13. C. J. Neiderud, How urbanization affects the epidemiology of emerging infectious diseases, *Infect. Ecol. Epidemiol.*, **5** (2015), 27060. https://doi.org/10.3402/iee.v5.27060

14. R. Reyes, R. Ahn, K. Thurber, T. F. Burke, Urbanization and infectious diseases: general principles, historical perspectives, and contemporary challenges, *Challenges Infect. Dis.*, (2013), 123–146. https://doi.org/10.1007/978-1-4614-4496-1_4

15. I. Frost, T. P. Van Boeckel, J. Pires, J. Craig, R. Laxminarayan, Global geographic trends in antimicrobial resistance: the role of international travel, *J. Travel Med.*, **26** (2019), taz036. https://doi.org/10.1093/jtm/taz036

16. A. C. Steere, J. Coburn, L. Glickstein, The emergence of Lyme disease, *J. Clin. Invest.*, **113** (2004), 1093–1101. https://doi.org/10.1172/JCI200421681

17. G. Dehner, Legionnaires' disease: Building a better world for you, *Environ. Hist.*, 2018. https://doi.org/10.1093/envhis/emy046

18. P. M. Schlievert, T. J. Tripp, M. L. Peterson, Reemergence of staphylococcal toxic shock syndrome in Minneapolis-St. Paul, Minnesota, during the 2000–2003 surveillance period, *J. Clin. Microbiol.*, **42** (2004), 2875–2876. https://doi.org/10.1128/JCM.42.6.2875–2876.2004

19. W. M. Lee, J. E. Polson, D. S. Carney, B. Sahin, M. Gale Jr, Reemergence of hepatitis C virus after 8.5 years in a patient with hypogammaglobulinemia: evidence for an occult viral reservoir, *J. Infect. Dis.*, **192** (2005), 1088–1092. https://doi.org/10.1086/432917

20. S. Sridhar, S. K. P. Lau, P. C. Y. Woo, Hepatitis E: A disease of reemerging importance, *J. Formosan Med. Assoc.*, **114** (2015), 681–690. https://doi.org/10.1016/j.jfma.2015.02.003

21. M. Pal, K. P. Gutama, Hantavirus disease: An emerging and re-emerging viral disease of public health concern, *Am. J. Infect. Dis.*, **12** (2024), 19–22. https://doi.org/10.12691/ajidm-12-1-4

22. M. T. P. Gilbert, A. Rambaut, G. Wlasiuk, T. J. Spira, A. E. Pitchenik, M. Worobey, The emergence of HIV/AIDS in the Americas and beyond, *Proc. Natl. Acad. Sci. U.S.A.*, **104** (2007), 18566–18570. https://doi.org/10.1073/pnas.070532910

23. T. W. Chun, R. T. Davey Jr, D. Engel, H. C. Lane, A. S. Fauci, Re-emergence of HIV after stopping therapy, *Nature*, **401** (1999), 874–875. https://doi.org/10.1038/44755

24. R. E. Baker, A. S. Mahmud, I. F. Miller, M. Rajeev, F. Rasambainarivo, B. L. Rice, et al., Infectious disease in an era of global change, *Nat. Rev. Microbiol.*, **20** (2022), 193–205. https://doi.org/10.1038/s41579-021-00639-z

25. H. Liao, C. J. Lyon, B. Ying, T. Hu, Climate change, its impact on emerging infectious diseases and new technologies to combat the challenge, *Emerging Microbes Infect.*, **13** (2024), 2356143. https://doi:10.1080/22221751.2024.2356143

26. S. P. Luby, J. Davis, R. R. Brown, S. M. Gorelick, T. H. F. Wong, Broad approaches to cholera control in Asia: Water, sanitation and handwashing, *Vaccine*, **38** (2020), A110–A117. https://doi.org/10.1016/j.vaccine.2019.07.084

27. G. Chowell, H. Nishiura, Transmission dynamics and control of Ebola virus disease (EVD): a review, *BMC Med.*, **12** (2014), 196. https://doi.org/10.1186/s12916-014-0196-0

28. G. Ledder, *Mathematical Modeling for Epidemiology and Ecology*, Springer Undergraduate Texts in Mathematics and Technology, Springer International Publishing, 2023.

29. H. W. Hethcote, The mathematics of infectious diseases, *SIAM Rev.*, **42** (2000), 599–653. https://doi.org/10.1137/S003614450037190

30. E. G. Nepomuceno, M. L. C. Peixoto, M. J. Lacerda, A. S. L. O. Campanharo, R. H. C. Takahashi, L. A. Aguirre, Application of optimal control of infectious diseases in a model-free scenario, *SN Comput. Sci.*, **2** (2021), 405. https://doi.org/10.1007/s42979-021-00794-3

31. O. Sharomi, T. Malik, Optimal control in epidemiology, *Ann. Oper. Res.*, **251** (2017), 55–71. https://doi.org/10.1007/s10479-015-1834-4

32. T. K. Kar, S. Jana, A theoretical study on mathematical modelling of an infectious disease with application of optimal control, *Biosystems*, **111** (2013), 37–50. https://doi.org/10.1016/j.biosystems.2012.10.003

33. S. Lenhart, J. T. Workman, *Optimal Control Applied to Biological Models*, Chapman and Hall/CRC, 2007. https://doi.org/10.1201/9781420011418

34. S. S. Musa, S. Qureshi, S. Zhao, A. Yusuf, U. T. Mustapha, D. He, Mathematical modeling of COVID-19 epidemic with effect of awareness programs, *Infect. Dis. Modell.*, **11** (2021), 448–460. https://doi.org/10.1016/j.idm.2021.01.012

35. H. Gaff, E. Schaefer, Optimal control applied to vaccination and treatment strategies for various epidemiological models, *Math. Biosci. Eng.*, **6** (2009), 469–492. https://doi.org/10.3934/mbe.2009.6.469

36. F. Lin, K. Muthuraman, M. Lawley, An optimal control theory approach to non-pharmaceutical interventions, *BMC Infect. Dis.*, **10** (2010), 1–13. https://doi.org/10.1186/1471-2334-10-32

37. D. Huremović, *Psychiatry of Pandemics: a Mental Health Response to Infection Outbreak*, Springer, (2019), 85–94. https://doi.org/10.1007/978-3-030-15346-5_8

38. S. Guerstein, V. Romeo-Aznar, M. Dekel, O. Miron, N. Davidovitch, R. Puzis, et al., The interplay between vaccination and social distancing strategies affects COVID-19 population-level outcomes, *PLoS Comput. Biol.*, **17** (2021), e1009319. https://doi.org/10.1371/journal.pcbi.1009319

39. R. Katz, A. Vaught, S. J. Simmens, Local decision making for implementing social distancing in response to outbreaks, *Public Health Rep.*, **134** (2019), 150–154. https://doi.org/10.1177/0033354918819755

40. G. Ledder, S. Manzoni, An optimal control problem for resource utilisation by microorganisms, *Int. J. Math. Educ. Sci. Technol.*, **55** (2024), 547–564. https://doi.org/10.1080/0020739X.2023.2254314

41. A. Keimer, L. Pflug, Modeling infectious diseases using integro-differential equations: optimal control strategies for policy decisions and applications in COVID-19, *Res Gate*, **10** (2020). https://doi.org/10.13140/RG.2.2.10845.44000

42. J. Mondal, S. Khajanchi, P. Samui, Impact of media awareness in mitigating the spread of an infectious disease with application to optimal control, *Eur. Phys. J. Plus*, **137** (2022), 983. https://doi.org/10.1140/epjp/s13360-022-03156-x

43. A. Rachah, A mathematical model with isolation for the dynamics of Ebola virus, in *Journal of Physics: Conference Series*, **1132** (2018), 012058. https://doi.org/10.1088/1742-6596/1132/1/012058

44. M. D. Ahmad, M. Usman, A. Khan, M. Imran, Optimal control analysis of Ebola disease with control strategies of quarantine and vaccination, *Infect. Dis. Poverty*, **5** (2016), 1–12. https://doi.org/10.1186/s40249-016-0161-6

45. E. Bonyah, K. Badu, S. K. Asiedu-Addo, Optimal control application to an Ebola model, *Asian Pac. J. Trop. Biomed.*, **6** (2016), 283–289. https://doi.org/10.1016/j.apjtb.2016.01.012

46. I. Area, F. Ndairou, J. J. Nieto, C. J. Silva, D. F. M. Torres, Ebola model and optimal control with vaccination constraints, preprint, arXiv:1703.01368.

47. G. Chowell, B. Cazelles, H. Broutin, C. V. Munayco, The influence of geographic and climate factors on the timing of dengue epidemics in Perú, 1994–2008, *BMC Infect. Dis.*, **11** (2011), 164. https://doi.org/10.1186/1471-2334-11-164

48. J. H. Arias-Castro, H. J. Martinez-Romero, O. Vasilieva, Biological and chemical control of mosquito population by optimal control approach, *Games*, **11** (2020), 62. https://doi.org/10.3390/g11040062

49. F. B. Agusto, M. A. Khan, Optimal control strategies for dengue transmission in Pakistan, *Math. Biosci.*, **305** (2018), 102–121. https://doi.org/10.1016/j.mbs.2018.09.007

50. M. A. L. Caetano, T. Yoneyama, Optimal and sub-optimal control in Dengue epidemics, *Optim. Control. Appl. Methods*, **22** (2001), 63–73. https://doi.org/10.1002/oca.683

51. K. P. Wijaya, T. Götz, E. Soewono, An optimal control model of mosquito reduction management in a dengue endemic region, *Int. J. Biomath.*, **7** (2014), 1450056. https://doi.org/10.1142/S1793524514500569

52. L. Lin, Y. Liu, X. Tang, D. He, The disease severity and clinical outcomes of the SARS-CoV-2 variants of concern, *Front. Public Health*, **9** (2021), 775224. https://doi.org/10.3389/fpubh.2021.775224

53. H. R. Sayarshad, An optimal control policy for COVID-19 pandemic until a vaccine deployment, *MedRxiv*, (2020), 2020-09. https://doi.org/10.1101/2020.09.26.20202325

54. G. A. Salcedo-Varela, F. Peñuñuri, D. González-Sánchez, S. Díaz-Infante, Synchronizing lockdown and vaccination policies for COVID-19: An optimal control approach based on piecewise constant strategies, *Optim. Control. Appl. Methods*, **45** (2024), 523–543. https://doi.org/10.1002/oca.3032

55. A. Rachah, Optimal control strategies for assessing the impact of medical masks on COVID-19 dynamics: global perspectives and societal well-being, *Open J. Social Sci.*, **12** (2024), 315–330. https://doi.org/10.4236/jss.2024.123022

56. H. Bohloli, H. R. Jamshidi, A. Ebraze, F. Rabbani Khah, Combining government, non-pharmaceutical interventions and vaccination in optimal control COVID-19, *Int. J. Healthcare Manage.*, **16** (2023), 61–69. https://doi.org/10.1080/20479700.2022.2071803

57. L. Mari, R. Casagrandi, E. Bertuzzo, D. Pasetto, S. Miccoli, A. Rinaldo, et al., The epidemicity index of recurrent SARS-CoV-2 infections, *Nat. Commun.*, **12** (2021), 2752. https://doi.org/10.1038/s41467-021-22878-7

58. J. C. Lemaitre, D. Pasetto, M. Zanon, E. Bertuzzo, L. Mari, S. Miccoli, et al., Optimal control of the spatial allocation of COVID-19 vaccines: Italy as a case study, *PLoS Comput. Biol.*, **18** (2022), e1010237. https://doi.org/10.1371/journal.pcbi.1010237

59. D. Louz, H. E. Bergmans, B. P. Loos, R. C. Hoeben, Emergence of viral diseases: mathematical modeling as a tool for infection control, policy and decision making, *Crit. Rev. Microbiol.*, **36** (2010), 195–211. https://doi.org/10.3109/10408411003604619

60. E. Jung, S. Iwami, Y. Takeuchi, T. Jo, Optimal control strategy for prevention of avian influenza pandemic, *J. Theor. Biol.*, **260** (2009), 220–229. https://doi.org/10.1016/j.jtbi.2009.05.031

61. S. Lee, G. Chowell, C. Castillo-Chávez, Optimal control for pandemic influenza: the role of limited antiviral treatment and isolation, *J. Theor. Biol.*, **265** (2010), 136–150. https://doi.org/10.1016/j.jtbi.2010.04.003

62. K. O. Okosun, R. Ouifki, N. Marcus, Optimal control strategies and cost-effectiveness analysis of a malaria model, *BioSystems*, **111** (2013), 83–101. https://doi.org/10.1016/j.biosystems.2012.09.008

63. W. Valega-Mackenzie, K. Ríos-Soto, S. Lenhart, Optimal control applied to Zika virus epidemics in Colombia and Puerto Rico, *J. Theor. Biol.*, **575** (2023), 111647. https://doi.org/10.1016/j.jtbi.2023.111647

64. H. R. Joshi, Optimal control of an HIV immunology model, *Optim. Control. Appl. Methods*, **23** (2002), 199–213. https://doi.org/10.1002/oca.710

65. S. Lee, G. Chowell, Exploring optimal control strategies in seasonally varying flu-like epidemics, *J. Theor. Biol.*, **412** (2017), 36–47. https://doi.org/10.1016/j.jtbi.2016.09.023

66. U. Ledzewicz, H. Maurer, H. Schättler, Bang-bang optimal controls for a mathematical model of chemo-and immunotherapy in cancer, *Discrete Contin. Dyn. Syst. - Ser. B*, **29** (2024), 1481–1500. https://doi.org/10.3934/dcdsb.2023141

67. G. Giordano, F. Blanchini, R. Bruno, P. Colaneri, A. Di Filippo, A. Di Matteo, et al., Modelling the COVID-19 epidemic and implementation of population-wide interventions in Italy, *Nat. Med.*, **26** (2020), 855–860. https://doi.org/10.1038/s41591-020-0883-7

68. J. M. Read, J. R. E. Bridgen, D. A. T. Cummings, A. Ho, C. P. Jewell, Novel coronavirus 2019-nCoV (COVID-19): early estimation of epidemiological parameters and epidemic size estimates, *Phil. Trans. R. Soc. B*, **376** (2021), 20200265. https://doi.org/10.1098/rstb.2020.0265

69. R. Dandekar, G. Barbastathis, Quantifying the effect of quarantine control in COVID-19 infectious spread using machine learning, *MedRxiv*, (2020), 2020-04. https://doi.org/10.1101/2020.04.03.20052084

70. D. Zou, L. Wang, P. Xu, J. Chen, W. Zhang, Q. Gu, Epidemic model guided machine learning for COVID-19 forecasts in the United States, *MedRxiv*, (2020), 2020-05. https://doi.org/10.1101/2020.05.24.20111989

71. J. T. Wu, K. Leung, G. M. Leung, Nowcasting and forecasting the potential domestic and international spread of the 2019-nCoV outbreak originating in Wuhan, China: a modelling study, *Lancet*, **395** (2020), 689–697. https://doi.org/10.1016/S0140-6736(20)30260-9

72. Z. Yang, Z. Zeng, K. Wang, S. S. Wong, W. Liang, M. Zanin, et al., Modified SEIR and AI prediction of the epidemics trend of COVID-19 in China under public health interventions, *J. Thoracic Dis.*, **12** (2020), 165. https://doi.org/10.21037/jtd.2020.02.64

73. A. Scherer, A. McLean, Mathematical models of vaccination, *Br. Med. Bull.*, **62** (2002), 187–199. https://doi.org/10.1093/bmb/62.1.187

74. B. Tang, X. Wang, Q. Li, N. L. Bragazzi, S. Tang, Y. Xiao, et al., Estimation of the transmission risk of the 2019-nCoV and its implication for public health interventions, *J. Clin. Med.*, **9** (2020), 462. https://doi.org/10.3390/jcm9020462

75. C. Tsay, F. Lejarza, M. A. Stadtherr, M. Baldea, Modeling, state estimation, and optimal control for the US COVID-19 outbreak, *Sci. Rep.*, **10** (2020), 10711. https://doi.org/10.1038/s41598-020-67459-8

76. R. Luo, A. D. Herrera-Reyes, Y. Kim, S. Rogowski, D. White, A. Smirnova, Estimation of time-dependent transmission rate for COVID-19 SVIRD model using predictor–corrector algorithm, in *Mathematical Modeling for Women's Health: Collaborative Workshop for Women in Mathematical Biology*, (2024), 213–237. https://doi.org/10.1007/978-3-031-58516-6

77. A. Smirnova, M. Baroonian, Reconstruction of incidence reporting rate for SARS-CoV-2 Delta variant of COVID-19 pandemic in the US, *Infect. Dis. Modell.*, **9** (2024), 70–83. https://doi.org/10.1016/j.idm.2023.12.001

78. Centers for Disease Control and Prevention, *United States COVID-19 Cases and Deaths by State over Time (ARCHIVED)*. Available from: https://data.cdc.gov/Case-Surveillance/United-States-COVID-19-Cases-and-Deaths-by-State-o/9mfq-cb36.

79. CDC, *Trends in Number of COVID-19 Vaccinations in the US*, 2022. Available from: https://covid.cdc.gov/covid-data-tracker/#vaccination-trends.

80. E. P. Esteban, L. Almodovar-Abreu, Assessing the impact of vaccination in a COVID-19 compartmental model, *Inf. Med. Unlocked*, **27** (2021), 100795. https://doi.org/10.1016/j.imu.2021.100795

81. M. Dashtbali, M. Mirzaie, A compartmental model that predicts the effect of social distancing and vaccination on controlling COVID-19, *Sci. Rep.*, **11** (2021), 8191. https://doi.org/10.1038/s41598-021-86873-0

82. A. Smirnova, M. Baroonian, X. Ye, Optimal epidemic control with nonmedical and medical interventions, *Mathematics*, **12** (2024), 2811. https://www.mdpi.com/2227-7390/12/18/2811

83. L. S. Pontryagin, *Mathematical Theory of Optimal Processes*, Routledge, 2018. https://doi.org/10.1201/9780203749319

84. A. Smirnova, X. Ye, On optimal control at the onset of a new viral outbreak, *Infect. Dis. Modell.*, **9** (2024), 995–1006. https://doi.org/10.1016/j.idm.2024.05.006

85. N. Tuncer, A. Timsina, M. Nuno, G. Chowell, M. Martcheva, Parameter identifiability and optimal control of a SARS-CoV-2 model early in the pandemic, *J. Biol. Dyn.*, **16** (2022), 412–438. https://doi.org/10.1080/17513758.2022.2078899

86. M. L. Diagne, F. B. Agusto, H. Rwezaura, J. M. Tchuenche, S. Lenhart, Optimal control of an epidemic model with treatment in the presence of media coverage, *Sci. Afr.*, **24** (2024), e02138. https://doi.org/10.1016/j.sciaf.2024.e02138

87. E. Howerton, K. Dahlin, C. J. Edholm, L. Fox, M. Reynolds, B. Hollingsworth, et al., The effect of governance structures on optimal control of two-patch epidemic models, *J. Math. Biol.*, **87** (2023), 74. https://doi.org/10.1007/s00285-023-02001-8

88. U. Ledzewicz, H. Schättler, On optimal singular controls for a general SIR-model with vaccination and treatment, in *Conference Publications*, **2011** (2011), 981–990. https://doi.org/10.3934/proc.2011.2011.981

89. P. E. Parham, J. Waldock, G. K. Christophides, D. Hemming, F. Agusto, K. J. Evans, et al., Climate, environmental and socio-economic change: weighing up the balance in vector-borne disease transmission, *Philos. Trans. R. Soc. London, Ser. B*, **370** (2015), 20130551. http://dx.doi.org/10.1098/rstb.2013.0551

90. J. A. Patz, P. Daszak, G. M. Tabor, A. A. Aguirre, M. Pearl, J. Epstein, et al., Unhealthy landscapes: policy recommendations on land use change and infectious disease emergence, *Environ. Health Perspect.*, **112** (2004), 1092–1098. https://doi.org/10.1289/ehp.68
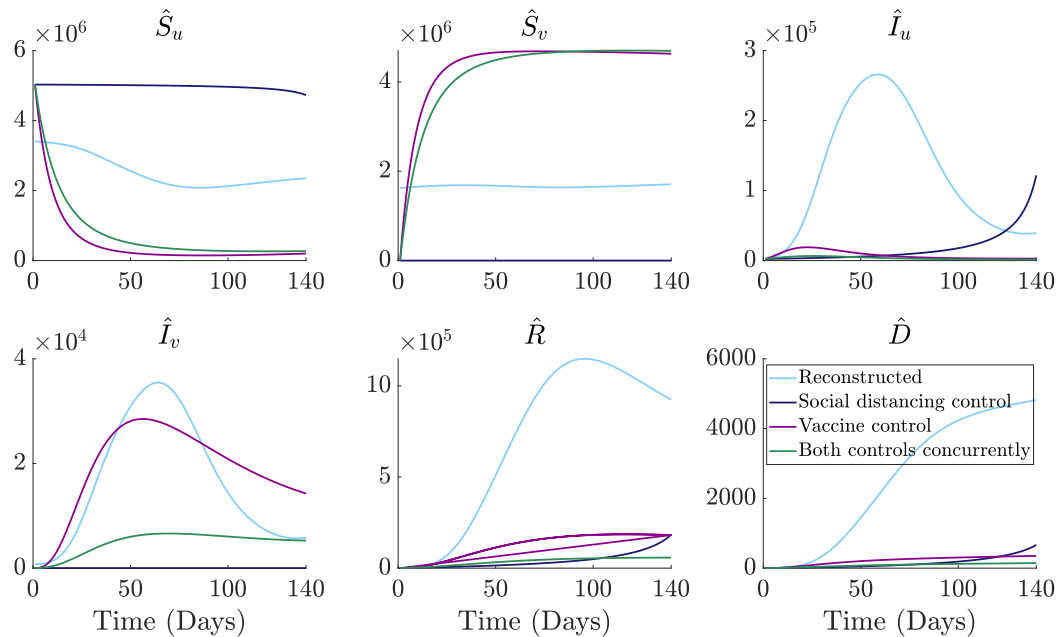
Appendix

Figure A1. Comparison of "social distancing control", "vaccine control", and "both controls concurrently" scenarios in Alabama using $\lambda_1 = 0.01$ and $c_{i,1}(u)$, $i = 1, 2$, as defined in (2.8) vs. the corresponding state variables reconstructed from real data from July 9, 2021 to November 25, 2021 [78].

Table A1. Comparison of $\hat{I}_u + \hat{I}_v$ for "no control", "social distancing control", "vaccine control", "both controls concurrently", and "reconstructed" scenarios in the state of Alabama using $\lambda_1 = 0.01$ and $c_{i,1}(u)$, $i = 1, 2$, as defined in (2.8).

Time	No control	Social distancing	Vaccine control	Both controls	Reconstructed
1	2371	2371	2371	2371	2371
10	40,696	2765	13,973	5136	12,931
20	727,429	3287	28,523	8069	57,315
30	2,141,225	3924	36,564	9924	146,430
40	1,339,108	4709	39,028	10,686	232,932
50	705,677	5684	38,244	10,701	284,223
60	415,208	6916	35,889	10,302	300,622
70	289,554	8512	32,910	9717	278,744
80	240,857	10,629	29,829	9085	223,886
90	235,218	13,525	26,908	8482	159,736
100	259,258	17,694	24,275	7948	107,825
110	304,815	24,126	21,979	7502	73,895
120	363,137	35,093	20,028	7155	54,193
130	412,240	57,058	18,410	6911	45,048
140	437,274	121,705	17,105	6774	45,207

Figure A2. Comparison of "social distancing control", "vaccine control", and "both controls concurrently" scenarios in Maryland using $\lambda_1 = 0.01$ and $c_{i,1}(u)$, $i = 1, 2$, as defined in (2.8) vs. the corresponding state variables reconstructed from real data from July 9, 2021 to November 25, 2021 [78].

Table A2. Comparison of $\hat{I}_u + \hat{I}_v$ for "no control", "social distancing control", "vaccine control", "both controls concurrently", and "reconstructed" scenarios in the state of Maryland using $\lambda_1 = 0.01$ and $c_{i,1}(u)$, $i = 1, 2$, as defined in (2.8).

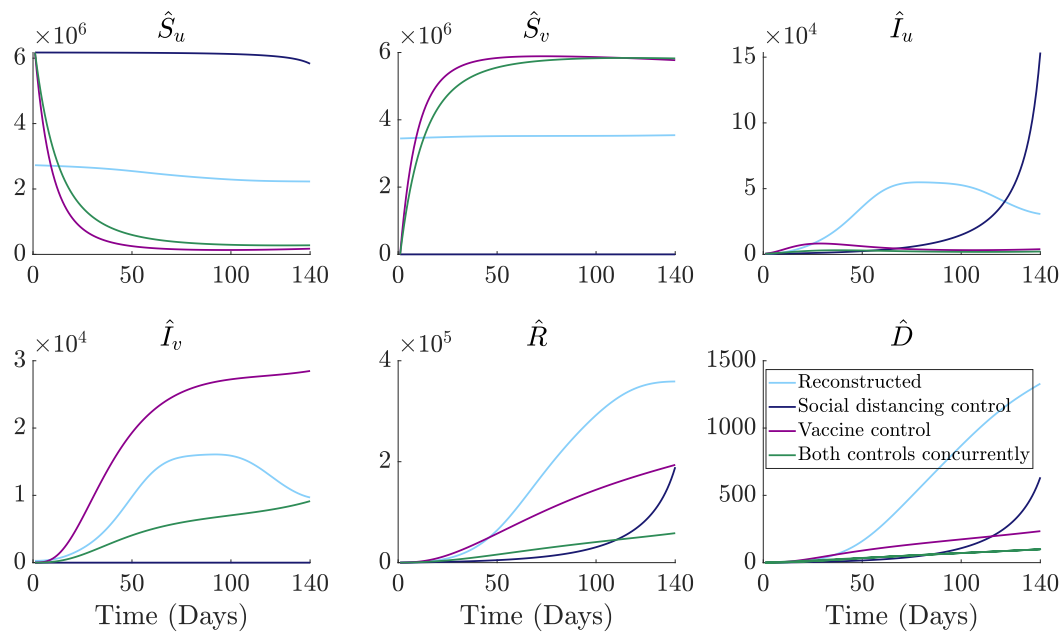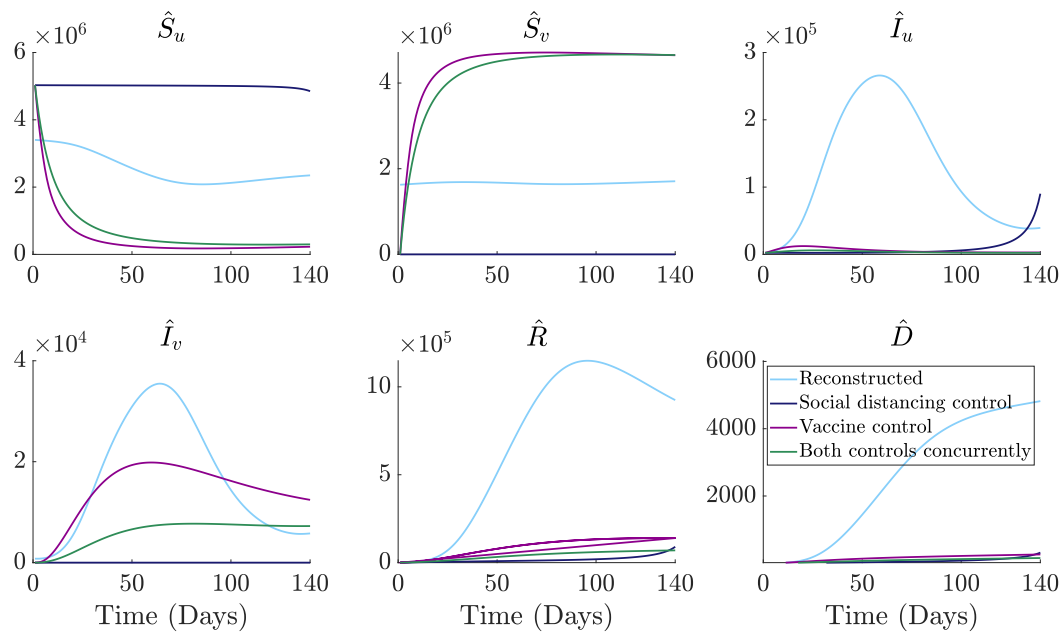| Time	No control	Social distancing	Vaccine control	Both controls	Reconstructed
1	481	481	481	481	481
10	14,918	649	4245	1507	1985
20	560,240	905	11,361	3145	6593
30	2,909,568	1263	17,781	4779	14,952
40	1,761,357	1765	22,409	6090	28,291
50	894,572	2470	25,516	7028	45,862
60	523,511	3469	27,536	7667	61,363
70	372,472	4902	28,818	8105	69,079
80	321,317	6987	29,623	8420	70,707
90	326,022	10,070	30,135	8687	70,354
100	368,754	14,801	30,493	8967	68,577
110	434,214	22,503	30,811	9313	63,308
120	499,860	36,206	31,185	9779	54,496
130	541,285	64,797	31,699	10,422	45,721
140	547,813	153,529	32,442	11,322	40,418

Figure A3. Comparison of "social distancing control", "vaccine control", and "both controls concurrently" scenarios in Alabama using $\lambda_1 = 0.01$ and $c_{i,2}(u)$, $i = 1, 2$, as defined in (2.8) vs. the corresponding state variables reconstructed from real data from July 9, 2021 to November 25, 2021 [78].

Table A3. Comparison of $\hat{I}_u + \hat{I}_v$ for "no control", "social distancing control", "vaccine control", "both controls concurrently", and "reconstructed" scenarios in the state of Alabama using $\lambda_1 = 0.01$ and $c_{i,2}(u)$, $i = 1, 2$, as defined in (2.8).

Time	No control	Social distancing	Vaccine control	Both controls	Reconstructed
1	2371	2371	2371	2371	2371
10	40,696	2274	11,635	4847	12,931
20	727,429	2224	20,152	7737	57,315
30	2,141,225	2237	24,705	9759	146,430
40	1,339,108	2317	26,414	10,879	232,932
50	705,677	2465	26,429	11,338	284,223
60	415,208	2702	25,487	11,367	300,622
70	289,554	3072	24,044	11,150	278,744
80	240,857	3640	22,412	10,819	223,886
90	235,218	4519	20,809	10,464	159,736
100	259,258	5958	19,350	10,129	107,825
110	304,815	8556	18,065	9846	73,895
120	363,137	13,951	16,961	9643	54,193
130	412,240	28,069	16,043	9538	45,048
140	437,274	90,177	15,304	9547	45,207

Figure A4. Comparison of "social distancing control", "vaccine control", and "both controls concurrently" scenarios in Maryland using $\lambda_1 = 0.01$ and $c_{i,2}(u)$, $i = 1, 2$, as defined in (2.8) vs. the corresponding state variables reconstructed from real data from July 9, 2021 to November 25, 2021 [78].

Table A4. Comparison of $\hat{I}_u + \hat{I}_v$ for "no control", "social distancing control", "vaccine control", "both controls concurrently", and "reconstructed" scenarios in the state of Maryland using $\lambda_1 = 0.01$ and $c_{i,2}(u)$, $i = 1, 2$, as defined in (2.8).

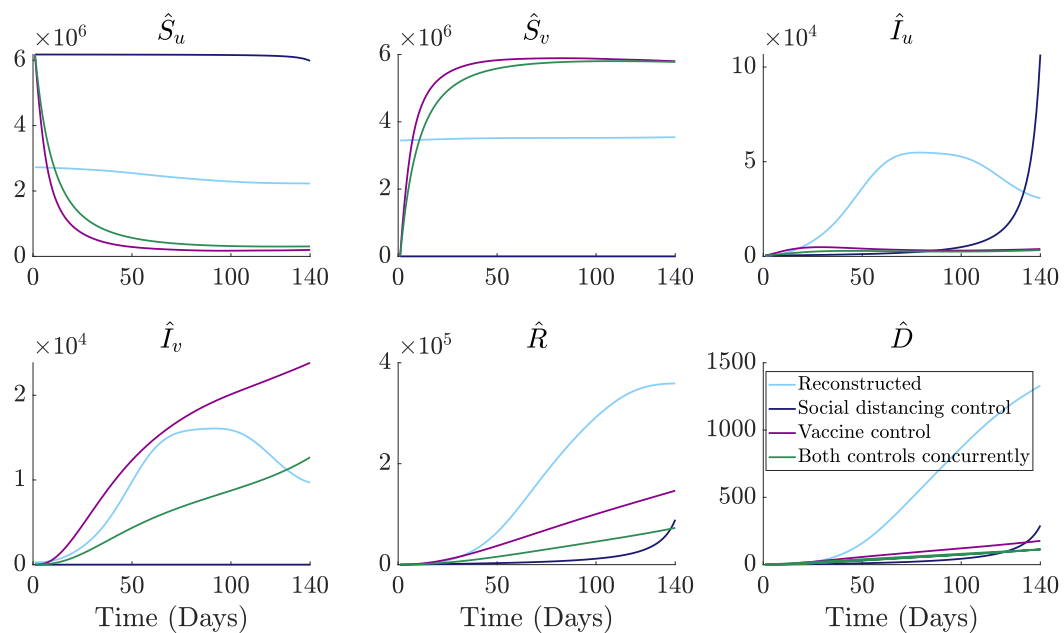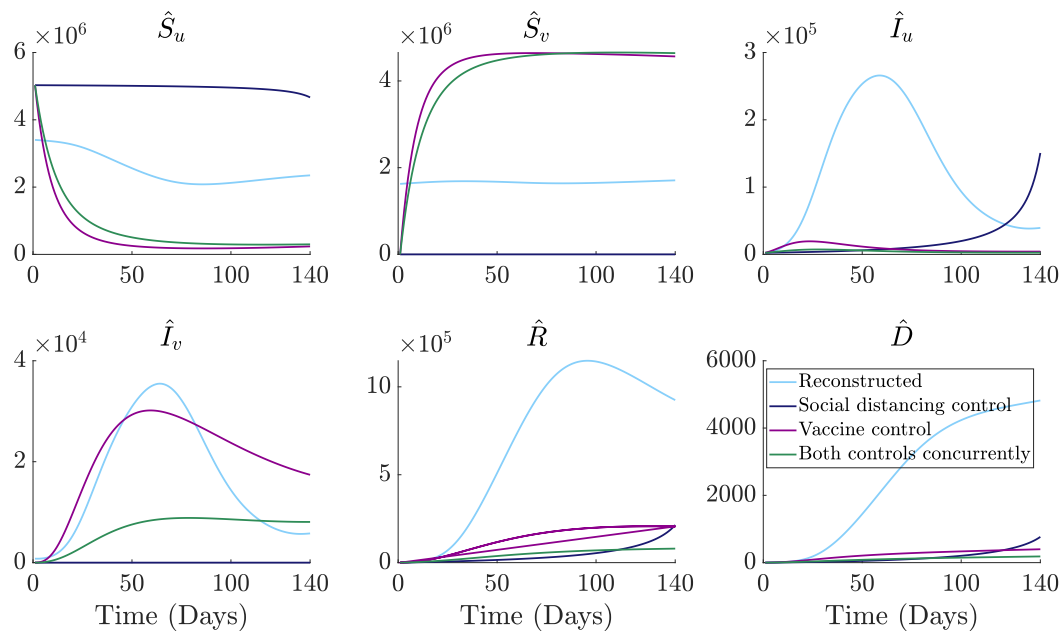| Time	No control	Social distancing	Vaccine control	Both controls	Reconstructed
1	481	481	481	481	481
10	14,918	560	3433	1434	1985
20	560,240	666	7565	2988	6593
30	2,909,568	802	11,214	4593	14,952
40	1,761,357	975	14,142	6019	28,291
50	894,572	1201	16,439	7219	45,862
60	523,511	1501	18,293	8214	61,363
70	372,472	1919	19,827	9056	69,079
80	321,317	2524	21,106	9809	70,707
90	326,022	3441	22,189	10,538	70,354
100	368,754	4917	23,184	11,298	68,577
110	434,214	7601	24,205	12,144	63,308
120	499,860	13,299	25,293	13,153	54,496
130	541,285	28,853	26,441	14,407	45,721
140	547,813	106,619	27,738	16,011	40,418

Figure A5. Comparison of "social distancing control", "vaccine control", and "both controls concurrently" scenarios in Alabama using $\lambda_1 = 0.01$ and $c_{i,3}(u)$, $i = 1, 2$, as defined in (2.8) vs. the corresponding state variables reconstructed from real data from July 9, 2021 to November 25, 2021 [78].

Table A5. Comparison of $\hat{I}_u + \hat{I}_v$ for "no control", "social distancing control", "vaccine control", "both controls concurrently", and "reconstructed" scenarios in the state of Alabama using $\lambda_1 = 0.01$ and $c_{i,3}(u)$, $i = 1, 2$, as defined in (2.8).

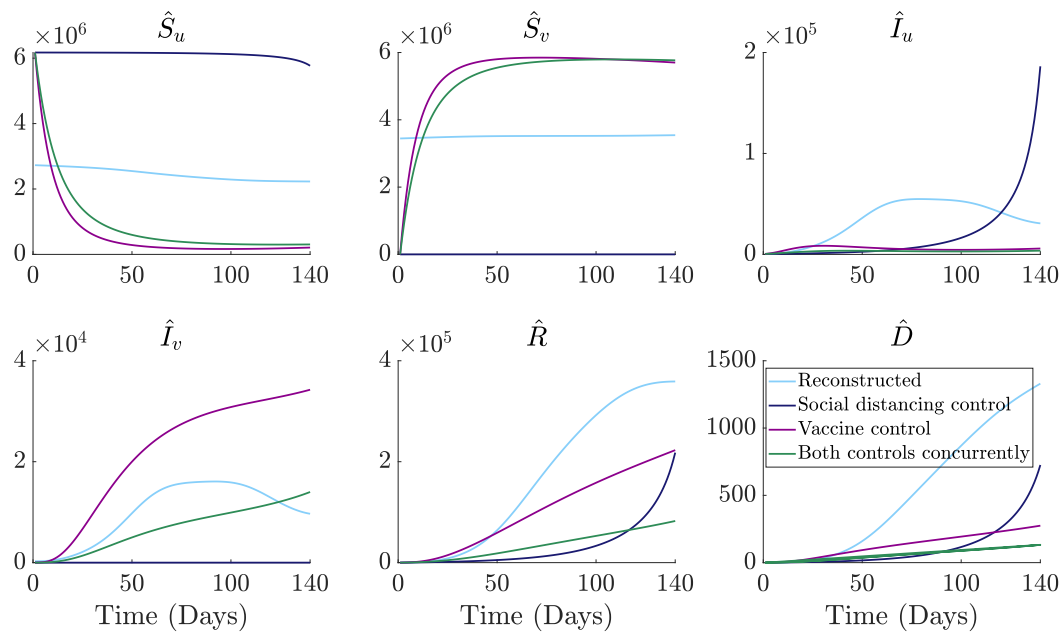| Time	No control	Social distancing	Vaccine control	Both controls	Reconstructed
1	2371	2371	2371	2371	2371
10	40,696	2803	13,971	5378	12,931
20	727,429	3379	28,783	8922	57,315
30	2,141,225	4089	37,551	11,494	146,430
40	1,339,108	4971	40,905	12,892	232,932
50	705,677	6072	40,915	13,397	284,223
60	415,208	7470	39,159	13,344	300,622
70	289,554	9291	36,585	12,989	278,744
80	240,857	11,721	33,758	12,500	223,886
90	235,218	15,064	30,992	11,983	159,736
100	259,258	19,865	28,452	11,507	107,825
110	304,815	27,365	26,223	11,111	73,895
120	363,137	40,312	24,336	10,823	54,193
130	412,240	66,979	22,795	10,658	45,048
140	437,274	150,695	21,595	10,634	45,207

Figure A6. Comparison of "social distancing control", "vaccine control", and "both controls concurrently" scenarios in Maryland using $\lambda_1 = 0.01$ and $c_{i,3}(u)$, $i = 1, 2$, as defined in (2.8) vs. the corresponding state variables reconstructed from real data from July 9, 2021 to November 25, 2021 [78].

Table A6. Comparison of $\hat{I}_u + \hat{I}_v$ for "no control", "social distancing control", "vaccine control", "both controls concurrently", and "reconstructed" scenarios in the state of Maryland using $\lambda_1 = 0.01$ and $c_{i,3}(u)$, $i = 1, 2$, as defined in (2.8).

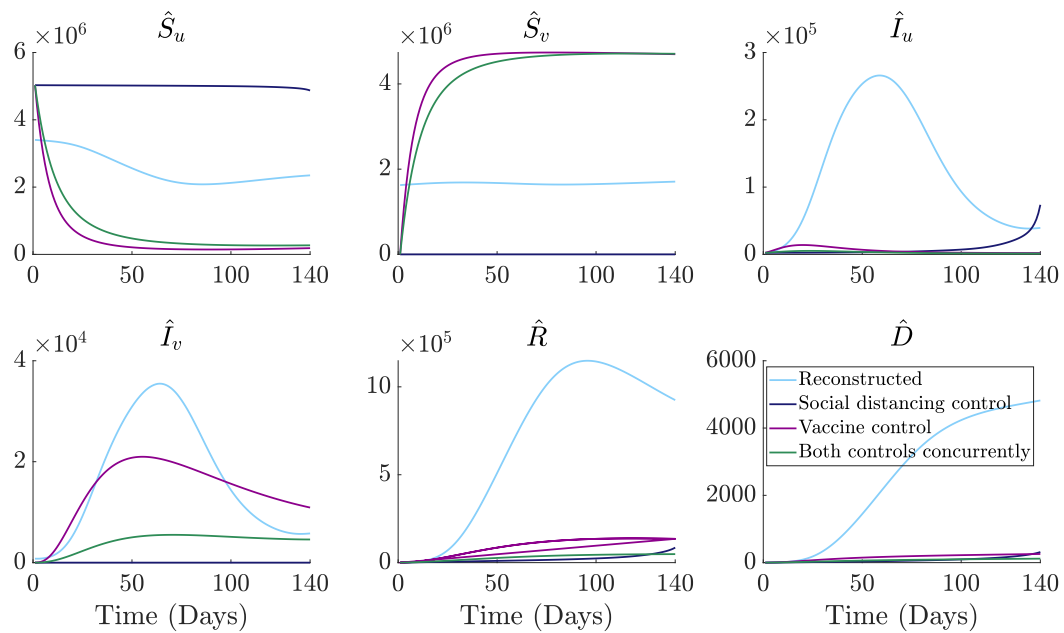| Time	No control	Social distancing	Vaccine control	Both controls	Reconstructed
1	481	481	481	481	481
10	14,918	656	4232	1562	1985
20	560,240	925	11,383	3411	6593
30	2,909,568	1306	18,083	5400	14,952
40	1,761,357	1846	23,243	7153	28,291
50	894,572	2611	27,017	8568	45,862
60	523,511	3703	29,746	9689	61,363
70	372,472	5284	31,731	10,596	69,079
80	321,317	7605	33,208	11,366	70,707
90	326,022	11,066	34,365	12,084	70,354
100	368,754	16,401	35,352	12,827	68,577
110	434,214	25,165	36,301	13,671	63,308
120	499,860	40,981	37,331	14,692	54,496
130	541,285	74,655	38,555	15,985	45,721
140	547,813	186,325	40,086	17,671	40,418

Figure A7. Comparison of "social distancing control", "vaccine control", and "both controls concurrently" scenarios in Alabama using $\lambda_1 = 0.01$ and $c_{i,4}(u)$, $i = 1, 2$, as defined in (2.8) vs. the corresponding state variables reconstructed from real data from July 9, 2021 to November 25, 2021 [78].

Table A7. Comparison of $\hat{I}_u + \hat{I}_v$ for "no control", "social distancing control", "vaccine control", "both controls concurrently", and "reconstructed" scenarios in the state of Alabama using $\lambda_1 = 0.01$ and $c_{i,4}(u)$, $i = 1, 2$, as defined in (2.8).

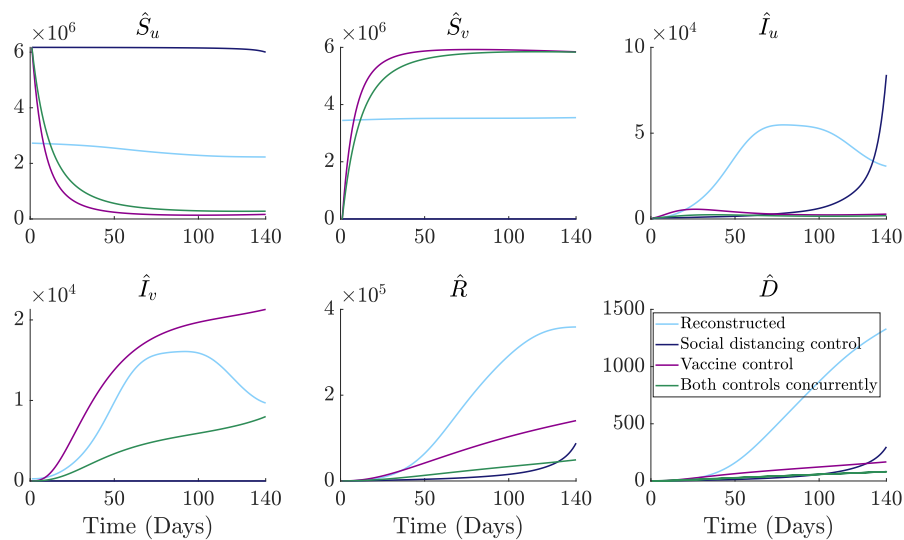| Time	No control	Social distancing	Vaccine control	Both controls	Reconstructed
1	2371	2371	2371	2371	2371
10	40,696	2439	12,420	4515	12,931
20	727,429	2504	22,394	6729	57,315
30	2,141,225	2638	27,163	8090	146,430
40	1,339,108	2860	28,380	8646	232,932
50	705,677	3108	27,669	8664	284,223
60	415,208	3427	26,027	8388	300,622
70	289,554	3932	24,013	7978	278,744
80	240,857	4698	21,931	7531	223,886
90	235,218	5721	19,936	7097	159,736
100	259,258	7158	18,113	6695	107,825
110	304,815	9768	16,497	6372	73,895
120	363,137	15,072	15,100	6139	54,193
130	412,240	25,394	13,915	5961	45,048
140	437,274	73,684	12,927	5894	45,207

Figure A8. Comparison of "social distancing control", "vaccine control", and "both controls concurrently" scenarios in Maryland using $\lambda_1 = 0.01$ and $c_{i,4}(u)$, $i = 1, 2$, as defined in (2.8) vs. the corresponding state variables reconstructed from real data from July 9, 2021 to November 25, 2021 [78].

Table A8. Comparison of $\hat{I}_u + \hat{I}_v$ for "no control", "social distancing control", "vaccine control", "both controls concurrently", and "reconstructed" scenarios in the state of Maryland using $\lambda_1 = 0.01$ and $c_{i,4}(u)$, $i = 1, 2$, as defined in (2.8).

Time	No control	Social distancing	Vaccine control	Both controls	Reconstructed
1	481	481	481	481	481
10	14,918	716	3746	1345	1985
20	560,240	835	8772	2655	6593
30	2,909,568	1075	12,890	3917	14,952
40	1,761,357	1312	15,846	4928	28,291
50	894,572	1574	17,903	5672	45,862
60	523,511	1991	19,336	6206	61,363
70	372,472	2623	20,347	6606	69,079
80	321,317	3422	21,076	6932	70,707
90	326,022	4450	21,625	7228	70,354
100	368,754	6172	22,074	7538	68,577
110	434,214	9392	22,491	7909	63,308
120	499,860	15,181	22,941	8389	54,496
130	541,285	28,291	23,468	9022	45,721
140	547,813	83,997	24,124	9914	40,418

AIMS Press